Fine Chemical Engineering
http://ojs.wiserpub.com/index.php/FCE/

Research Article

Box-Behnken Design for MAFM Precision Surface Finishing of Al-6063/SiC/B_4C Composites: A Comparative Study with Nature-Inspired Algorithms

Gagandeep Chawla[1*], Rishi Sarup Sharma[1], Vinod Kumar Mittal[2]

[1]Department of Mechanical Engineering, Seth Jai Parkash Mukand Lal Institute of Engineering and Technology, Radaur-135133, Yamunanagar, Haryana, India
[2]Department of Mechanical Engineering, National Institute of Technology, Kurukshetra-136119, Haryana, India
E-mail: gagandeepchawla@jmit.ac.in

Received: 14 June 2024; **Revised:** 10 October 2024; **Accepted:** 17 October 2024

Graphical abstract:

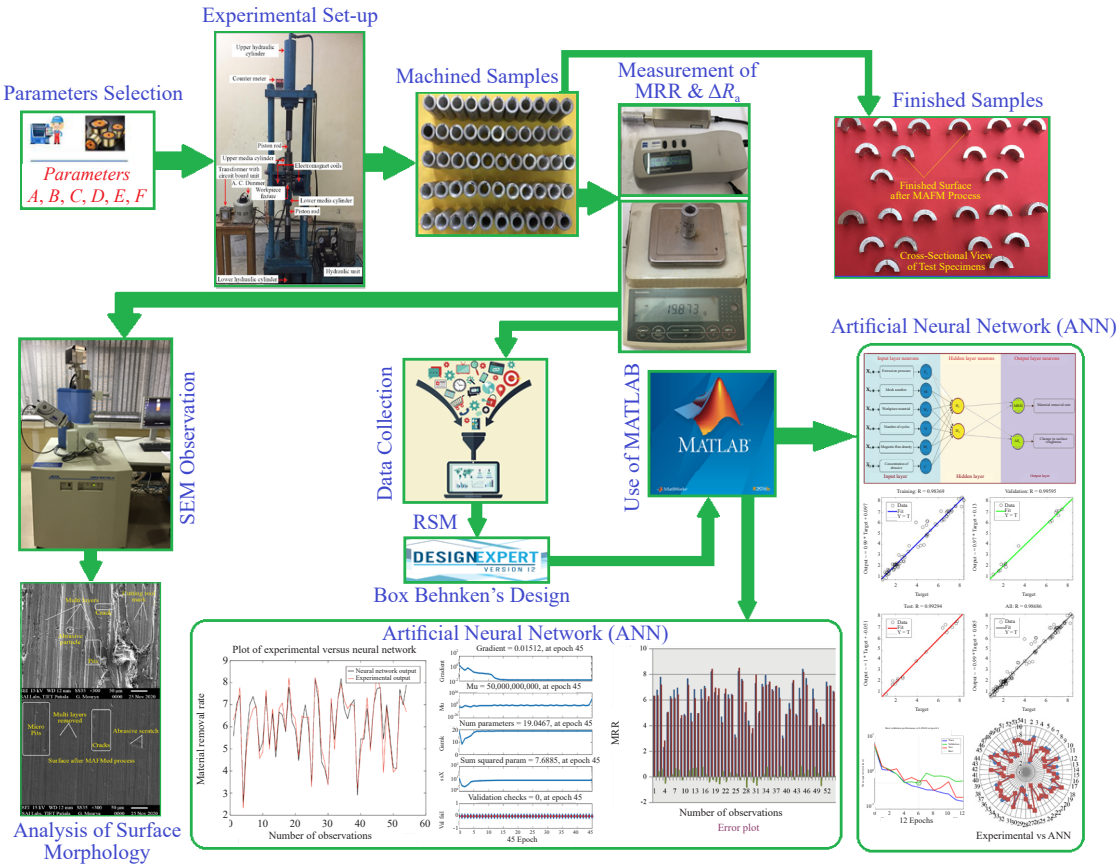

Schematic of the experimental set-up with methodologies proposed

DOI: https://doi.org/10.37256/fce.6120255137

Abstract: Precision polishing is difficult for advanced materials like silicon carbide and boron carbide. Magnetic abrasive flow machining (MAFM) has become an effective method for cleaning, deburring, and polishing metal and high-tech engineering parts. By finishing hybrid Al/SiC/B_4C-metal matrix composites (MMCs), this research uses MAFM for experimental readings. The present work is innovative due to the aluminum workpiece fixture, hybrid composites, and response surface methodology (RSM) modeling. The neural simulation of the MAFM process and nature-inspired error reduction make it unique. Using six input and two output parameters, a generic framework is created. Box-Behnken design (BBD) of response surface methodology plans and executes 54 runs of experimentation. The hybrid artificial neural network (ANN) technique is used to compare the MAFM process systematically. ANN is used to model parameter input-output relations. To anticipate the created surface accurately, regression models must be precise. These hybrid particle swarm optimization (PSO)-genetic algorithm (GA)-simulated annealing (SA) algorithms optimize the MAFM process. Additionally, trained ANN models outperform the BBD model in prediction. For optimal error reduction, the neural network uses Bayesian regularization with 112 iterations. The ANN model regression graph shows a correlation between inputs and outputs. A scanning electron microscope (SEM) with 300-magnification examines the workpiece surface. According to SEM, MAFM provides fine surface textures, thus reducing abnormalities.

***Keywords*:** magnetic abrasive flow machining, Al/SiC/B_4C composites, precision polishing, response surface methodology, hybrid artificial neural network

Abbreviations

MAFM	Magnetic abrasive flow machining
ANN	Artificial neural networks
RSM	Response surface methodology
MRR	Material removal rate
BBD	Box-Behnken design
MMCs	Metal matrix composites
SEM	Scanning electron microscope
Trainbr	Bayesian regularization training algorithm
MSE	Mean square error
ΔR_a	Change in surface roughness
PSO	Particle Swarm Optimization
PS	Pattern Search
GA	Genetic Algorithm
SA	Simulated Annealing

1. Introduction

Magnetic abrasive flow machining (MAFM) is one of the novel non-traditional machining approaches that excels in finishing off difficult-to-reach component regions. Precision components are successfully deburred, radiused, and recast layers removed using this technique. For a variety of parts, high levels of surface polish and adequate close tolerances have been attained.[1] A semi-solid media comprising of abrasives and polymer-based carrier, is pushed across the machining surfaces in abrasive flow machining (AFM) under pressure. During a restriction, the media behaves as a deformable grinding tool. To direct the media to the proper areas in the workpiece, a specific fixture is typically needed. The AFM process was developed by Extrude Hone Corporation in the United States during the 1960's. Several empirical researches have been carried out since then.[1-5] Williams and Rajurkar,[6] gained insights into process mechanisms, process monitoring, and surface generation modeling of AFM in the late 1980s. Their study mainly focused on stochastic process modeling and online supervision of AFM via acoustic emission.[7] The impact of the machining operation on the surface quality created by AFM and the process was analyzed by Loveless and Kozak et al.[8-9] Studies on the rheological

characteristics and impact of temperature of media in AFM were suggested by Fletcher and others.[10-11] SiC/Al-MMCs surfaces were examined by Wang et al.[12] using the wire electrical discharge machining (WEDM) technique. Przyklenk[13] carried out parametric analysis on the AFM setup. Using the finite elements in neural simulation, various researchers focused their study on the removal of material, mathematical modeling along with the generation of surface.[14-16] To reduce the WEDM surface roughness, Wang and Weng introduced a more affordable and efficient abrasive media.[17] A silicone-based polymer was blended with abrasive particles to generate a flexible media, selected as a carrier for this purpose. AFM was used by Sankar et al.[18] to generate various media from abrasives, plasticizers and styrene butadiene-based polymers. Rotational abrasive flow finishing was employed to carry out the experiments for finishing Al alloy and its MMCs to study the impact of storage, modulus of stress relaxation, percentage viscous component and shear stress on ΔR_a and MRR as separate parameters.

According to Steif and Haan,[19] the existence of "dispersive stresses" facilitates surface wear during AFM. In order to machine blind cavities, Jones and Hull[20] modified the current AFM by using ultrasonic vibrations in the medium. It is claimed that Gilmore's orbital flow machining method is superior to AFM.[21] These procedures fall under the category of hybrid machining processes (HMP), a relatively new idea developed in the area of non-traditional machining. Ahmad et al.[22] finished Ti-6Al-4V/Titanium (Grade-5) material by conducting the experimentation on DC based magnetic abrasive finishing (MAF) setup. The input-output parameters were modeled using ANNs. For reducing/optimizing the MAF process errors, genetic algorithms (GAs) were employed. Sharma et al.[23] aimed to develop a Box-Behnken design (BBD) model with a three-level factorial design for various parameters to predict the ΔR_a of Al-6061/SiC/Al_2O_3/rare earth oxides (REOs) hybrid composites. Oh and Lee[24] conducted an analysis of data from force sensors and acoustic emission to predict the surface finish in the MAF process using ANN. Djavanroodi[25] utilized ANN modeling to predict the surface roughness of the MAF process.

Neural networks were utilized for surface roughness parameter prediction by El-Sonbaty et al.[26] and Abburi et al.[27] Jain et al. optimized the AFF process using ANN and evolutionary algorithms.[28] The findings obtained using the ANN model and the projected machined surface quality and MRR values were found to be in good agreement. Lam and Smith[29] investigated the cascade-correlation neural network methodology for modeling the AFF and it was superior to the back-propagation technique. Teimouri et al.[30] developed the adaptive neuro-fuzzy inference system (ANFIS) and feed forward back-propagation neural network (FFBP-NN) to forecast the performance of the MAF process. To increase the rate of finishing and material removal, Sankar et al.[31] proposed rotating the medium along its axis. To perform parametric analysis and fully comprehend the drill bit-guided abrasive flow finishing (DBG-AFF) process, modeling employing non-linear multi-variable regression analysis and ANN is used. The neural network simulation data exhibit good agreement with the experimental outcomes.

Jain and Jain[32] employed neural networks for modeling to make the best possible choice of AFM process input parameters. The effectiveness of this approach has been validated by AFM process optimization data generated using genetic algorithms. Around fifteen such procedures have been reported by Rajurkar and Kozak.[33] A lower rate of material removal is a common issue in most of the novel machining procedures (such as electrochemical machining, electric discharge machining and laser beam machining, etc.). Shinmura and Yamaguchi,[34] and more recently Kremen et al.,[35] Kim et al.,[36] Khairy,[37] and Shan et al.[38] have reported studies on the MAFM process.

The primary stimulus for using MAFM is to overcome the limitations of conventional abrasive flow machining (AFM). Traditional AFM often struggles with low material removal rates and suboptimal surface finishes due to the ineffective engagement of abrasive particles with the workpiece. MAFM addresses these challenges by utilizing a variable magnetic field to enhance the movement and interaction of abrasives, thereby improving machining efficiency and quality, especially for complex geometries and hard-to-reach areas.

The MAFM process has several benefits, including increased material removal rate, better surface finish, accessibility to complex geometries, decreased tool wear, and versatility. However, there are also some drawbacks, including complicated setup, higher initial costs, magnetic field limitation, operational restrictions, and the possibility of abrasive agglomeration.

The current study utilizes the neural network approach to simulate the MAFM process, as presented by different researchers, by way of utilizing various simulation techniques. The feed-forward and back-propagation configurations of the neural network ensure stability and are capable of modeling real-time systems, apart from bearing good approximation abilities. The prominent research papers have been included in the tabular form in Table 1, to showcase

the findings on a comparative basis. The table clearly illustrates the changes in the choice of material used, the research findings as well as the types of workpiece material and the methodology adopted. The gaps have been identified from the research papers, and the same has been employed to devise the methodology for the current research work.

In the present study, an attempt has been made to optimize the MRR and ΔR_a, by using the nature-inspired optimization techniques of simulated annealing (SA), particle swarm optimization (PSO) and genetic algorithm (GA). These methods help to minimize the mean square error (MSE) and thus facilitate better and more efficient modelling. The neural modeling is done with an emphasis on optimizing the response parameters like the MRR and ΔR_a.

Table 1. Literature-based comparison of finishing parameters and optimization techniques

Authors	Workpiece material	Abrasive/ Abrasive size	Type of magnetic source	Voltage or current supply	Machining gap/mm	Magnet flux density	Rotational speed/RPM	Remarks
Chaurasia et al.[39]	AZ91 magnesium alloy	Alumina/600# (~ 25.7 µm) Iron particle/320# (~ 50 µm)	Permanent magnet	0.4-0.8 A	1-2	0-0.35 T	90-220	Employs MAF using AZ91 magnesium alloy plate for the finishing process.
Kataria et al.[40]	Al/Al_2O_3 MMCs	Iron particle	Cylindrical-shaped poles	10 V 8 A	-	-	-	Grey relational analysis (GRA) is employed for obtaining machining parameters.
Kumar et al.[41]	SS316L	SiC/800#	Permanent magnet	1.25-2.25 V	0-2	0.22 T	30-150	It utilizes the RSM to investigate the process performance using COMSOL Multi-physics software, which is based on FEM analysis.
Sirwal et al.[42]	Ferro-magnetic P20 tool steel	SiC/800#, 1,000# Electrolytic iron particle/ 400#-1,200#	Permanent magnet	-	2	0.58-0.61 T	300-1,500	RSM design method is used for experimentation and process parameters are analysed through ANOVA.
Zhang et al.[43]	Rubber stern bearing	NBR particles	Permanent magnet	-	-	10.0-50.0 mT	200	Reynolds equation calculates the lubrication performance of the test rig using process parameters, and the solution is obtained through the finite difference method.
Singh et al.[44]	Aluminium 6060	SiC iron powder	-	10-18 V	1-2	0.65-1.02 T	100-300	The mouth-flame optimization algorithm for optimizing the MAF parameters using the hybrid ANN is employed using the back-propagation algorithm.
Ali et al.[45]	Brass	Al_2O_3/180#	-	0-16 A	0.25	-	100-300	The thermal additive centrifugal AFM process takes a simulation model of ANSYS to predict its MRR.

Table 1. (cont.)

Authors	Workpiece material	Abrasive/ Abrasive size	Type of magnetic source	Voltage or current supply	Machining gap/mm	Magnet flux density	Rotational speed/RPM	Remarks
Heng et al.[46]	SUS 316L	Fe powder/ #200 µm Al_2O_3 & iron-based composite abrasives/ #320 µm	Permanent magnet	-	-	0.41-0.48 T	50-600	It takes the aluminium and iron-based composites on the MAF process along with an ANN model to compute and simulate the surface roughness.
Verma et al.[47]	Stainless steel (SS304)	Ferromagnetic abrasive brush/ 400#-1,200#	Permanent magnet	-	-	0.4-0.8 T	200-600	The MAF process is applied for the surface finish of SS304 pipes are simulated using the Maxwell software.
Azizi et al.[48]	Inconel 718 (super alloy)	SiC/1,000# (15 µm) Iron particles	Electric magnet poles	-	1, 0.5	0.14 T	2,000, 1,500, 1,000	The MAF process has been investigated on Inconel 718 shaft for studying the effects of surface roughness and feed rate.
Judal et al.[49]	Aluminium	Al_2O_3/#1,200 (12.67 µm), #800 (19 µm), #600 (25.33 µm) Ferromagnetic/ #100 (152 µm)	DC supply	0.5-2 A	1.25	0.29-0.58 T	250, 420, 710, 1,200	The surface finishing of aluminium workpiece is studied using MAF process, leading to low-energy consumptions.
Kala et al.[50]	Copper alloy (C70600)	Al_2O_3/#600, #800, #1,000, #1,200 Fe powder/#300	DC supply	70-100 V	2	0.15 T	112, 140, 180, 224	The MAF process is employed for machining the non-ferrous materials in an efficient manner, with a view to investigate the effect of surface roughness on the workpiece material.
Kala et al.[51]	Copper alloy	Alumina/#800 Iron powder (#300)	Permanent magnet (Magnetic disks)	-	1.5-2.5	50-650 mT	200-400	The MAF process has been investigated using the ANOVA and Taguchi L_9 array with the experimental data.

2. Material and methods

2.1 *MAFM experimental set-up*

The setup for experimental analysis (Figure 1(a)) has been taken up after making the necessary changes in design and tested under laboratory conditions.

Figure 1(b) demonstrates the diagrammatic depiction of the MAFM process mechanism through the CAD model. The process variables may be varied in the setup for instance the extrusion pressure is allowed to vary till 10 MPa. The material required for the hydraulic cylinders was EN8. The diameter of 90 mm for the internal cylinder, stroke length of 250 mm and hydraulic oil no. 68 was taken. The workpiece fixture is made of aluminium, which is a non-magnetic material. It is specifically made to accept electromagnet poles so that the workpiece's inner surface experiences the

greatest magnetic force.

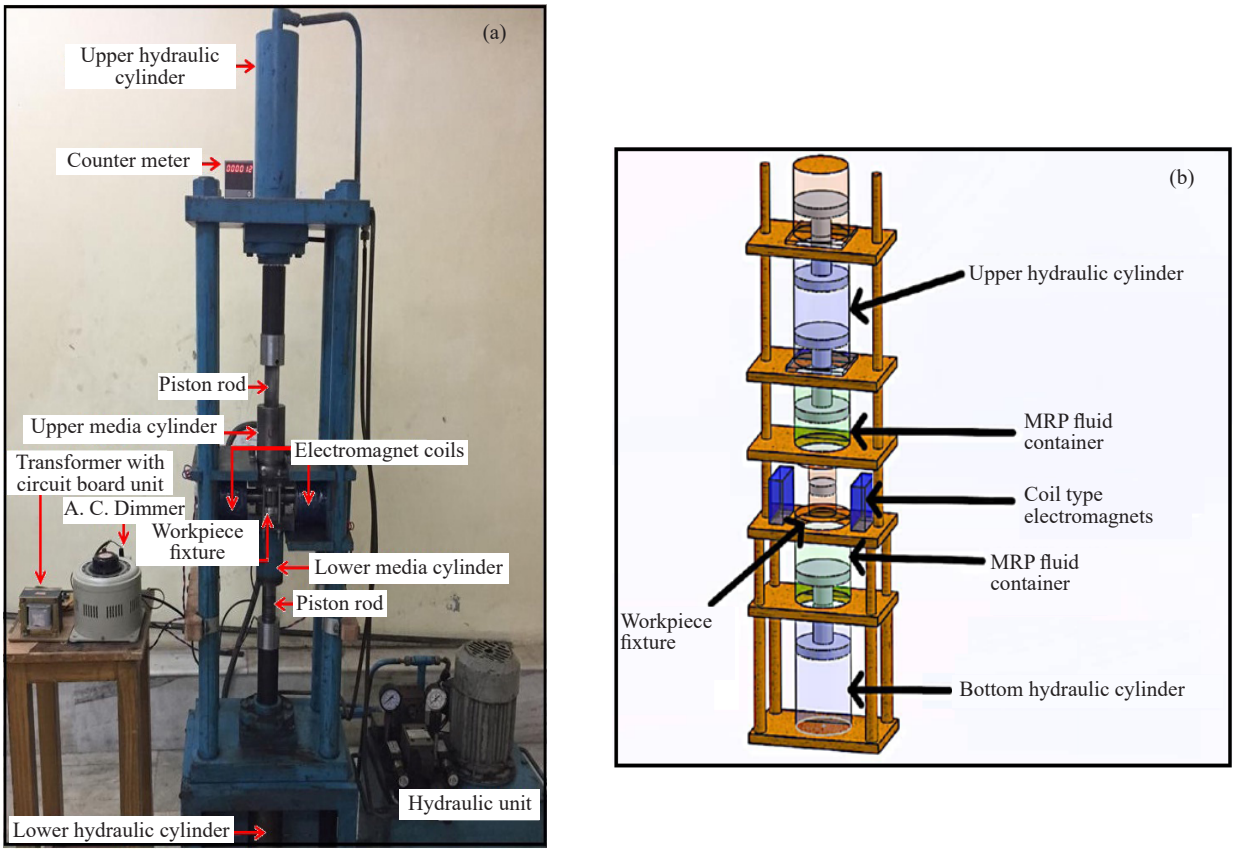

Figure 1. (a) Pictorial view of MAFM set-up. (b) CAD model shows the mechanism of MAFM

An aluminium fixture with slots is employed for holding the workpiece, as depicted in Figures 2(a) and 2(b). The intended use of such a fixture is to facilitate machinability, thus allowing for the slots to be accurately aligned with the shape of the workpiece. The cross-section of passage is reduced gradually to enable smooth passing of medium with a reduced vibration. Two plates have been attached in the fixture enabling variation in the vertical axis for holding the medium in a tight manner.

The coil-type electromagnet has been fabricated in its location surrounding the cylindrical workpiece. It comprises two poles which are enclosed by the coils. These poles are arranged so as to provide the presence of a strong magnetic field near the periphery of the workpiece. Table 2 enlists the specifications for the electromagnet.

The medium under consideration comprises polymer based on silicon (white color RTV-2615), hydraulic oil (68 nos.), and abrasive grains. The abrasive considered for this experiment must primarily be magnetic in nature. The medium has been run through a dummy workpiece two or three times, in order to accomplish a thorough mixing. Material removal has been accomplished using a loosely bonded magnetic abrasive medium composed of silicon carbide (SiC) and the experiments have been carried out on an MAFM experimental setup. The different compositions of constituents used for preparing the media for the MAFM process are depicted in Table 3. Upon the completion of desired cycles, the workpiece along with the fixture has been removed. Subsequently, another workpiece has been placed in the respective slots. A digital meter is employed to quantify the number of cycles. Acetone [$(CH_3)_2CO$] is applied to each finished sample for cleaning purposes.

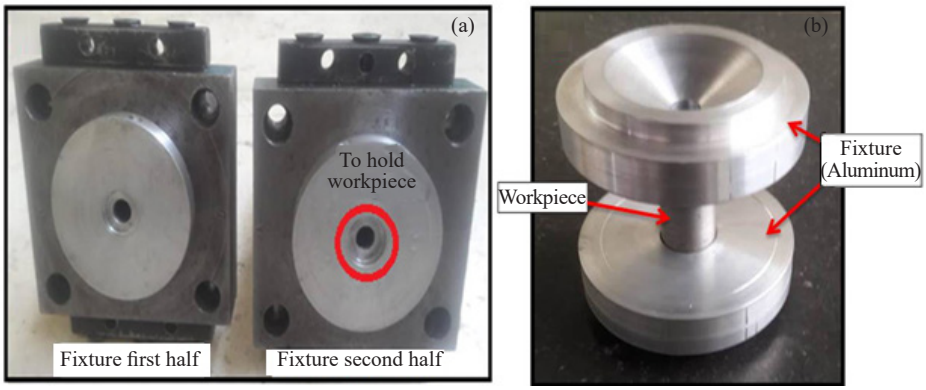

Figure 2. (a) Workpiece fixture, (b) Fixture holds the workpiece

Table 2. Coil type electromagnet specifications

Sr. No.	Constituents	Description
1.	Core material	Mild steel (M.S.)
2.	Core size	Core length = 175 mm Core radius = 25 mm Core rod diameter = 35 mm
3.	Electromagnet coils	Copper wire, 23 gauge, ϕ 0.5733 mm No. of turns = 2,500 per coil, Coil weight = 3.820 kg
4.	Power supply (DC)	0-240 V
5.	Magnetic flux density (M_f)	0.15 T 0.3 T 0.45 T
6.	Current applied (Amp.)	1.3 2.0 2.5

Table 3. Composition of magnetic abrasive media

Sr. No.	Constituents	Value of the constituents	% Volume concentration in media
1.	Silicon carbide (SiC) abrasive particle	150 mesh size 220 mesh size 400 mesh size	45%, 50%, 55%
2.	Iron (Fe) particle	300 mesh size	10%
3.	Hydraulic oil	68 number	10%
4.	Liquid silicon rubber	White colour (RTV-2615)	35%, 30%, 25%

2.2 *Mechanism of material removal in MAFM*

There are many ideas that attempt to explain how abrasive particles cause abrasion.[52-54] With specific modifications, Finnie's solid particle erosion theory has been acknowledged as a crucial component in the material removal process during the machining by AFM process.[52] Due to the medium stream's high speed during the machining using an abrasive jet, the abrasive particles that strike possess more energy. However, in AFM, strong pressure applied on the viscoelastic carrier media supplies the necessary energy to the abrasive particles. Due to the pressure operating in the

restriction, the abrasive particles and the medium dilates experience significant strain. The surface that is in contact with the abrasive is micro-ploughed and micro-chipped by the momentum that abrasive particles gain in these circumstances. The metal's surface experiences plastic deformation as a result of micro-ploughing. No material is subjected to initial erosion, but as time goes on, the surface atoms grow more susceptible to being stripped away by succeeding abrasive grains. Repeated strikes by more abrasive particles on the surface result in material separation. A common term for this is "cutting wear". Applying a strong magnetic field around the edge of the workpiece causes the abrasive particles in motion to undergo a sideways pull, which redirects their path. Surface micro-chipping happens when they impinge at a slight angle on the work surface. Abrasive distribution patterns at the machining surface as the workpiece are predicted to be impacted by the magnetic field as well. As a result, particles that would have previously flown by without touching the surface now follow a different path. Material removal has been improved as these particles play an active role in the process of abrasion. Even though the magnetic field's mechanical pull is weak, this is enough for deflecting the abrasive particles. These particles are pacing at high velocity. So, it appears that a greater quantity of abrasive particles hit the surface when a magnetic field is applied. At the same time, some of them make little angles as they impact the surface. As a result, cutting wear is enhanced. Consequently, it leads to an overall improvement in the material removal rate. The mechanism of material removal during the process of MAFM is depicted in Figure 3.

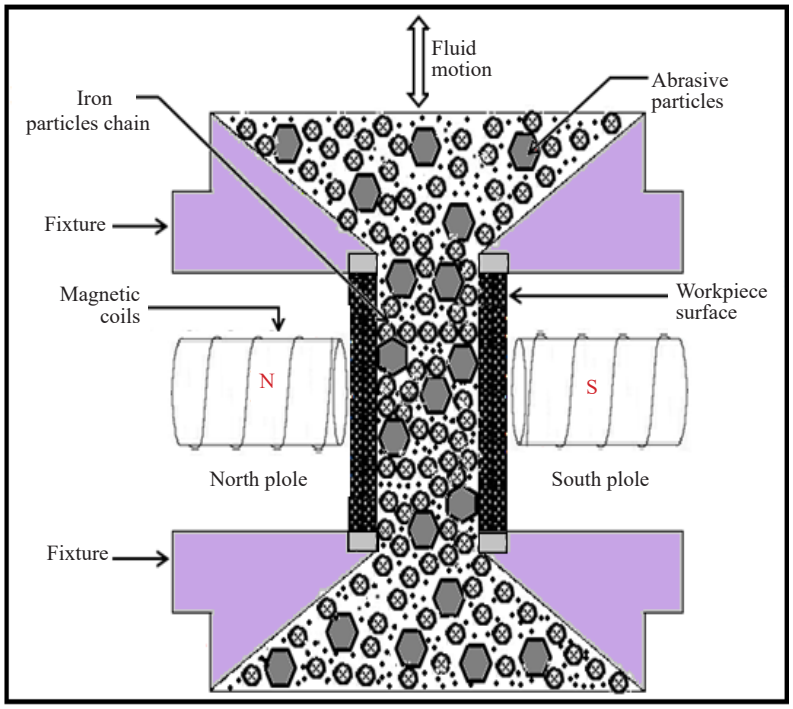

Figure 3. MAFM mechanism

2.3 *Methodology and design of experiments*

The design approach of Box-Behnken method related to RSM[55-57] is applicable to the experimental design as depicted in Table 4.

RSM technique is applied to simulate the relationship between the machining parameters. The purpose of the analysis is to investigate the impact of the parameters on the efficiency of the model. The design approach is implemented using the model equation and expressed as:

$$y = \beta_0 + \sum_{i=1}^{k} \beta_i x_i + \sum_{i=1}^{k} \beta_{ii} x_i^2 + \sum_{i<j} \beta_{ij} x_i x_j \quad (1)$$

Here y refers to the preferred response. $x_{i\ (1,\ 2,\ \ldots,\ k)}$ are the independent k quantitative process parameters, β_0 is a constant and, β_i, β_{ii} and β_{ij} are the coefficients of linear, quadratic and interaction terms, respectively. Design Expert® (6.0.8 version) software has been employed for computing the process variables' effect values on MRR and ΔR_a. The RSM model is developed at 95% confidence level. Terms having 'Prob > F' less than 0.05 are considered as significant. A two-way MAFM set-up, conceived and designed in-house, has been used for the experiments. Experimental investigation has been done for Al/SiC/B_4C-hybrid MMCs with different percentages of SiC (9, 8, and 7%), B_4C (1, 2, and 3%) and aluminum-6063 as base material. The element's percentage composition is depicted in Table 5.

Table 4. Design of experiments and results

Run No.	Extrusion pressure (E_p)	Mesh No. (M)	Concentration of abrasives (C)	Type of work material (W_p)	Number of cycles (N)	Magnetic flux density (M_f)	MRR (μg/s)	ΔR_a (μm)
1	5	220	45	1	150	0.15	6.31	1.52
2	7	400	50	1	150	0.3	6.78	2.24
3	5	150	55	2	200	0.3	7.78	2.68
4	3	400	50	3	150	0.3	2.32	0.79
5	3	150	50	1	150	0.3	5.01	1.42
6	5	220	50	2	150	0.3	6.28	1.73
7	7	220	50	1	100	0.3	6.79	1.91
8	5	400	55	2	200	0.3	6.94	2.21
9	3	400	50	1	150	0.3	4.56	1.31
10	7	220	50	3	100	0.3	4.87	1.72
11	5	150	45	2	200	0.3	7.66	2.51
12	3	220	55	2	150	0.45	4.97	1.39
13	5	400	45	2	200	0.3	6.82	1.98
14	5	220	45	3	150	0.45	4.94	1.73
15	5	220	45	1	150	0.45	6.83	1.98
16	5	400	50	2	100	0.45	7.08	2.19
17	7	220	50	3	200	0.3	5.87	2.13
18	7	220	50	1	200	0.3	8.21	2.79
19	5	400	50	2	200	0.15	6.58	1.27
20	5	400	45	2	100	0.3	6.35	1.81
21	3	220	45	2	150	0.15	4.68	1.12
22	5	220	55	1	150	0.15	6.49	1.65
23	5	220	50	2	150	0.3	6.42	1.75

Table 4. (cont.)

Run No.	Extrusion pressure (E_p)	Mesh No. (M)	Concentration of abrasives (C)	Type of work material (W_p)	Number of cycles (N)	Magnetic flux density (M_f)	MRR (μg/s)	ΔR_a (μm)
24	5	400	55	2	100	0.3	6.45	1.87
25	3	220	50	3	200	0.3	3.29	1.07
26	7	220	55	2	150	0.45	8.24	2.83
27	5	150	50	2	100	0.45	7.62	2.74
28	5	220	55	3	150	0.45	5.02	1.96
29	5	220	55	3	150	0.15	4.37	1.38
30	3	150	50	3	150	0.3	3.37	1.01
31	5	150	50	2	200	0.15	7.29	2.15
32	3	220	50	1	200	0.3	4.98	1.38
33	5	400	50	2	200	0.45	7.23	2.41
34	7	220	45	2	150	0.45	7.93	2.61
35	5	150	45	2	100	0.3	7.2	2.01
36	5	150	50	2	100	0.15	6.82	1.89
37	5	220	50	2	150	0.3	7.05	2.01
38	5	220	55	1	150	0.45	6.95	2.29
39	3	220	50	3	100	0.3	3.21	0.73
40	3	220	45	2	150	0.45	4.89	1.21
41	5	400	50	2	100	0.15	5.74	1.03
42	5	150	55	2	100	0.3	7.32	2.17
43	3	220	50	1	100	0.3	4.91	1.19
44	5	220	50	2	150	0.3	6.93	1.76
45	5	150	50	2	200	0.45	8.41	2.88
46	7	150	50	1	150	0.3	7.69	2.68
47	7	400	50	3	150	0.3	3.93	1.91
48	5	220	50	2	150	0.3	6.86	1.89
49	7	150	50	3	150	0.3	5.28	2.1
50	3	220	55	2	150	0.15	3.95	1.13
51	5	220	45	3	150	0.15	4.12	1.19
52	7	220	45	2	150	0.15	7.41	2.16
53	5	220	50	2	150	0.3	7.11	2.15
54	7	220	55	2	150	0.15	6.68	2.23

Table 5. The weight percentage of material composition

Element	Al	Fe	Mg	Cu	Si	Zn	Mn	Pb	B	Cr	Ti
Workpiece-1	Balance	0.28	0.76	0.03	9.15	0.0010	0.0064	0.0025	1.01	0.0016	0.0096
Workpiece-2	Balance	0.16	0.53	0.02	8.02	0.0012	0.0050	0.0026	1.96	0.0021	0.0090
Workpiece-3	Balance	0.18	0.72	0.04	6.82	0.0012	0.0068	0.0027	2.86	0.0021	0.0091

The fabricated rods of different compositions were initially faced, drilled and reamed using a lathe machine. Finally, the samples were finished by the MAFM setup. Cylindrical workpieces made of Al/SiC/B_4C-hybrid MMCs were selected as the test specimen. The size of a cylindrical workpiece is taken as external diameter (20 mm), internal diameter (12.5 mm) and length (40 mm) as depicted in Figures 4(a) and 4(b), on the basis of the guidelines.[38] Some finished specimens are shown in Figure 5.

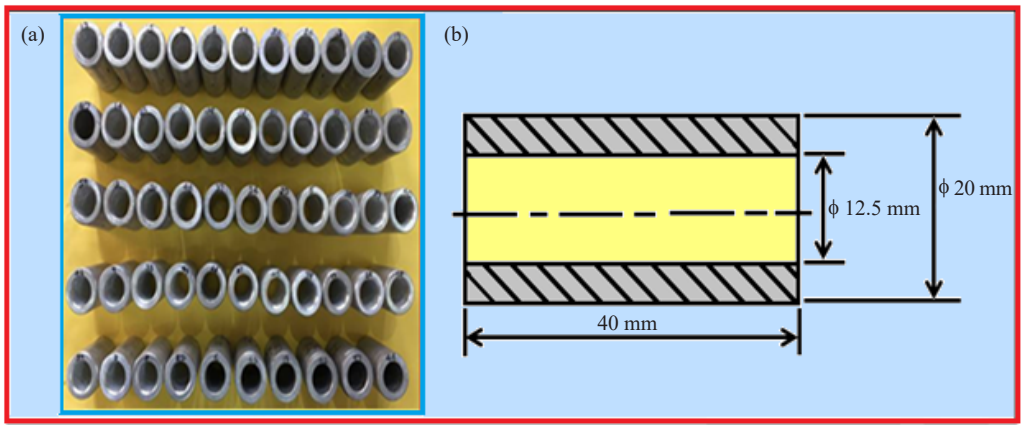

Figure 4. (a) Finished workpieces, (b) Job profile

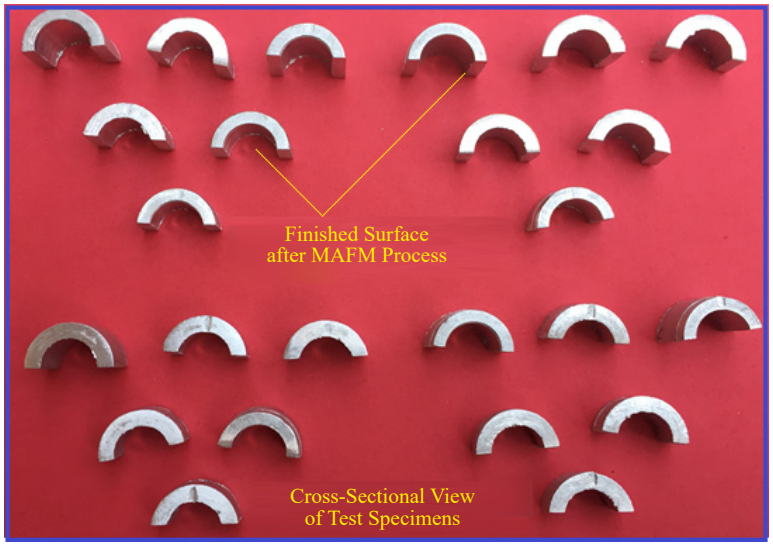

Figure 5. Finished workpieces after MAFM process

The weight and surface roughness of every sample is computed before and after each trial. Electronic balance BL-220H, with an accuracy of 10^{-3} g, is employed to measure the sample weight. The surface roughness of both the initial and final samples is measured using a digital handy surface roughness tester E35-B. The values of surface roughness were computed by taking the average of the readings at various surface points. Pilot experimental work was done by employing the one-variable-at-a-time (OVAT) approach with Al/SiC/B_4C-MMCs as workpieces. Extrusion pressure (E_p), mesh number (M), concentration of abrasives (C), workpiece material (W_p), number of cycles (N) and magnetic flux density (M_f) are taken as input process parameters. The MRR and ΔR_a were taken as the response parameters. The factors were adopted based upon the exhaustive literature review and pilot experimentation and their levels are depicted in Table 6.

Table 6. Factors with their levels (actual and coded)

Parameter	Symbols	Units	Lower range	Upper range	Coded low	Coded high	Mean	SD
A	E_p	MPa	3.00	7	–1 ↔ 3	+1 ↔ 7	5.00	1.35
B	M	Number	150	400	–1 ↔ 150	+1 ↔ 400	244.44	88.52
C	C	Wt. %	45	55	–1 ↔ 45	+1 ↔ 55	50.00	3.36
D	W_p	type	1	3	–1 ↔ 1	+1 ↔ 3	2.00	0.6729
E	N	-	100	200	–1 ↔ 100	+1 ↔ 200	150.00	33.65
F	M_f	Tesla	0.15	0.45	–1 ↔ 0.15	+1 ↔ 0.45	0.3000	0.1009

A total of 54 runs were conducted at stipulated conditions using the RSM technique.[58] The results (obtained through Design Expert® (6.0.8 version) software) have been compared with a newly created model having a bio-inspired neural network algorithm. In general, nature-inspired algorithms are used for fine tuning of the industrial systems, either in terms of minimization of error or optimal tuning of controllers. The PSO is a population-based nature-inspired algorithm that utilizes the social behavior of the swarm of particles to search effectively to reach the optimal solution. Global and best particle positions are some of the characteristics that define these particles. These swarms of particles employ their velocity to move within the search space. The PSO approach was inspired by the way a school of finish or a flock of birds behaves. The simulated annealing (SA) method owes its widespread use to a metallurgical process. The SA relates to the heating of metal and then subsequently cooling in order to attain a minimum energy state. Developed by John Holland in the 1970s, genetic algorithms (GA) derive their abstraction of the problem information, using Darwin's theory of biological evolution. These incorporate the principles of natural selection for the fittest among all the candidates. GAs are advantageous as they do not take into consideration the problem information. At the same time, they do not correlate with the problem parameters. Genetic algorithms have the ability to deal with complex problems.

2.4 *Mathematical relations for MRR, ΔR_a, and C*

The mathematical expressions (2), (3) and (4), respectively, are used to evaluate the response characteristics MRR and ΔR_a and the abrasive concentration in the media.

2.4.1 *Material removal rate (MRR)*

MRR stands for the volume of specimen material removed from the surface during the process of MAFM finishing. At the beginning and end of each trial, the duration of each procedure is recorded, and the weight of the workpiece is calculated. Microgram per second (μg/sec) is the unit of measurement for this type of removal rate MRR.

Mathematically, MRR is determined as follows:

$$\text{MRR} = \frac{(\text{Initial weight} - \text{Final weight})}{\text{Time}} \quad (2)$$

2.4.2 *Change in surface roughness (ΔR_a)*

R_a of both initial and final specimens has been measured using the digital handy surf roughness machine, model E35-B. The ΔR_a is calculated in micrometers (μm).

Mathematically, ΔR_a is determined as follows:

$$\Delta R_a = R_a(\text{initial}) - R_a(\text{final}) \quad (3)$$

Where:

R_a (initial) and R_a (final) are the values of surface roughness before and after finishing procedures.

2.4.3 *The abrasive concentration (C) in media*

The abrasive concentration (C) in the media is calculated as follows:

$$\text{Abrasive concentration in media} = \frac{\text{Weight of the abrasives in media}}{(\text{Weight of the abrasives in media} + \text{Weight of the carrier media})} \times 100 \quad (4)$$

2.5 *Applications of AFM and its variants*

The AFM process is used to achieve a high-quality inner wall polishing of micro bores (diameter < 500 μm) of various miniature parts such as micro pumps, ink-jet printer nozzles, micro filters and fuel injectors. Furthermore, it improves the surface quality of the non-linear tube carriers, a component often utilized in the military and civil sectors for certain exit passages of important components. The finishing of free-form components to the nanometer level that is used in aerospace, electronics, turbine blades, optical and automobile components can also be achieved by the AFM process and its variants. Additionally, it finds wide applications in medical fields for finishing free-form surfaces (Knee joint implants) in biomedical and surgical instruments.[59-65]

3. Results and discussions

3.1 *Artificial neural network (ANN)*

Neural networks have been recognized as the versatile procedures that are employed for regression as classification problems. One kind of such network that is widely used is the feed-forward network. Such an architecture comprises layers of neurons, so connected that there exists a definite relation between neurons in each layer and its previous layer. This feed-forward configuration of a neural network is capable of approximating a broad range of functions. Due to these flexible characteristics, these are also termed as “universal approximators”.[66] The neural model comprises three neuron layers. Here, the first layer neurons pertain to input parameters. The input layer comprises six neurons that are akin to the input variables. The second layer forms the hidden layer. The next task is to determine the number of hidden layers and the quantity of neurons in these for multilayer perceptrons. The experimental tweaking of learning rate parameters employs a number of methods. This refers to simulating existing models along with training that employs algorithms such as the Bayesian Algorithm. In such case, a for-loop is employed to iterate over multiple configurations of ANN architecture. Thereafter, the mean square error (MSE) is computed. The neural model’s architecture is defined by the learning rate that corresponds to the lowest MSE value.

3.2 *Training of artificial neural network*

The MRR and ΔR_a values are obtained to correspond to the initial and final finished surfaces. These are then

modeled by using the neural network. The ANNs have been individually developed for preparing the model of MRR and ΔR_a. The present research focuses on modeling the process of MAFM that has been implemented by employing the ANN architecture. To accurately express its output in terms of input parameters, the neural model uses a feed-forward back propagation technique. Experimental data values have been trained through the neural model, the configuration of which is shown in Table 7.

Table 7. Experimental and ANN predicted results for MRR and ΔR_a

Run No.	Input parameters and their values						Experimental		ANN predicted		Error		Absolute error %	
	Extrusion pressure (E_p)	Mesh No. (M)	Conc. of abrasives (C)	Type of work material (W_p)	Number of cycles (N)	Magnetic flux density (M_f)	MRR (µg/s)	ΔR_a (µm)	MRR (µg/s)	ΔR_a (µm)	MRR (µg/s)	ΔR_a (µm)	MRR (µg/s)	ΔR_a (µm)
1	5	220	45	1	150	0.15	6.31	1.52	6.3035	2.0972	0.0065	-0.5772	0.10301	-37.974
2	7	400	50	1	150	0.3	6.78	2.24	6.3437	1.9609	0.4363	0.2791	6.4351	12.4598
3	5	150	55	2	200	0.3	7.78	2.68	7.1767	2.1018	0.6033	0.5782	7.7545	21.5746
4	3	400	50	3	150	0.3	2.32	0.79	2.812	1.014	-0.492	-0.224	-21.207	-28.354
5	3	150	50	1	150	0.3	5.01	1.42	5.0476	1.5966	-0.0376	-0.1766	-0.7505	-12.437
6	5	220	50	2	150	0.3	6.28	1.73	6.0937	2.0668	0.1863	-0.3368	2.96656	-19.468
7	7	220	50	1	100	0.3	6.79	1.91	6.1354	2.1064	0.6546	-0.1964	9.64065	-10.283
8	5	400	55	2	200	0.3	6.94	2.21	6.414	1.9686	0.526	0.2414	7.57925	10.9231
9	3	400	50	1	150	0.3	4.56	1.31	4.7999	2.0319	-0.2399	-0.7219	-5.261	-55.107
10	7	220	50	3	100	0.3	4.87	1.72	4.7657	2.0746	0.1043	-0.3546	2.14168	-20.616
11	5	150	45	2	200	0.3	7.66	2.51	7.157	1.9499	0.503	0.5601	6.56658	22.3147
12	3	220	55	2	150	0.45	4.97	1.39	4.2988	2.2508	0.6712	-0.8608	13.505	-61.928
13	5	400	45	2	200	0.3	6.82	1.98	6.1226	1.9592	0.6974	0.0208	10.2258	1.05051
14	5	220	45	3	150	0.45	4.94	1.73	4.9479	1.966	-0.0079	-0.236	-0.1599	-13.642
15	5	220	45	1	150	0.45	6.83	1.98	6.0776	1.9666	0.7524	0.0134	11.0161	0.67677
16	5	400	50	2	100	0.45	7.08	2.19	6.8954	1.9772	0.1846	0.2128	2.60734	9.71689
17	7	220	50	3	200	0.3	5.87	2.13	6.2676	1.9399	-0.3976	0.1901	-6.7734	8.92488
18	7	220	50	1	200	0.3	8.21	2.79	8.4127	1.9177	-0.2027	0.8723	-2.4689	31.2652
19	5	400	50	2	200	0.15	6.58	1.27	6.9458	1.9659	-0.3658	-0.6959	-5.5593	-54.795
20	5	400	45	2	100	0.3	6.35	1.81	6.8886	1.9812	-0.5386	-0.1712	-8.4819	-9.4586
21	3	220	45	2	150	0.15	4.68	1.12	4.2477	2.367	0.4323	-1.247	9.23718	-111.34
22	5	220	55	1	150	0.15	6.49	1.65	6.8583	2.8593	-0.3683	-1.2093	-5.6749	-73.291
23	5	220	50	2	150	0.3	6.42	1.75	6.0937	2.0668	0.3263	-0.3168	5.08255	-18.103
24	5	400	55	2	100	0.3	6.45	1.87	6.3684	2.2043	0.0816	-0.3343	1.26512	-17.877
25	3	220	50	3	200	0.3	3.29	1.07	3.0594	2.0373	0.2306	-0.9673	7.00912	-90.402

Table 7. (cont.)

Run No.	Input parameters and their values						Experimental		ANN predicted		Error		Absolute error %	
	Extrusion pressure (E_p)	Mesh No. (M)	Conc. of abrasives (C)	Type of work material (W_p)	Number of cycles (N)	Magnetic flux density (M_f)	MRR (µg/s)	ΔR_a (µm)	MRR (µg/s)	ΔR_a (µm)	MRR (µg/s)	ΔR_a (µm)	MRR (µg/s)	ΔR_a (µm)
26	7	220	55	2	150	0.45	8.24	2.83	8.4916	1.9787	-0.2516	0.8513	-3.0534	30.0813
27	5	150	50	2	100	0.45	7.62	2.74	7.4669	2.1746	0.1531	0.5654	2.00919	20.635
28	5	220	55	3	150	0.45	5.02	1.96	5.8292	2.0378	-0.8092	-0.0778	-16.12	-3.9694
29	5	220	55	3	150	0.15	4.37	1.38	4.0086	2.7685	0.3614	-1.3885	8.27002	-100.62
30	3	150	50	3	150	0.3	3.37	1.01	3.7901	2.492	-0.4201	-1.482	-12.466	-146.73
31	5	150	50	2	200	0.15	7.29	2.15	7.9561	2.1307	-0.6661	0.0193	-9.1372	0.89767
32	3	220	50	1	200	0.3	4.98	1.38	5.1189	2.0513	-0.1389	-0.6713	-2.7892	-48.645
33	5	400	50	2	200	0.45	7.23	2.41	7.0164	1.9602	0.2136	0.4498	2.95436	18.6639
34	7	220	45	2	150	0.45	7.93	2.61	7.1626	1.9596	0.7674	0.6504	9.67718	24.9195
35	5	150	45	2	100	0.3	7.2	2.01	7.4179	2.2182	-0.2179	-0.2082	-3.0264	-10.358
36	5	150	50	2	100	0.15	6.82	1.89	6.6944	1.1468	0.1256	0.7432	1.84164	39.3228
37	5	220	50	2	150	0.3	7.05	2.01	7.0937	2.0668	-0.0437	-0.0568	-0.6199	-2.8259
38	5	220	55	1	150	0.45	6.95	2.29	6.1282	2.0597	0.8218	0.2303	11.8245	10.0568
39	3	220	50	3	100	0.3	3.21	0.73	3.0021	0.777	0.2079	-0.047	6.47664	-6.4384
40	3	220	45	2	150	0.45	4.89	1.21	4.8918	1.986	-0.0018	-0.776	-0.0368	-64.132
41	5	400	50	2	100	0.15	5.74	1.03	5.2717	1.253	0.4683	-0.223	8.15854	-21.65
42	5	150	55	2	100	0.3	7.32	2.17	7.5247	2.0874	-0.2047	0.0826	-2.7964	3.80645
43	3	220	50	1	100	0.3	4.91	1.19	4.772	1.8913	0.138	-0.7013	2.81059	-58.933
44	5	220	50	2	150	0.3	6.93	1.76	6.0937	2.0668	0.8363	-0.3068	12.0678	-17.432
45	5	150	50	2	200	0.45	8.41	2.88	8.1814	1.958	0.2286	0.922	2.71819	32.0139
46	7	150	50	1	150	0.3	7.69	2.68	7.159	1.9973	0.531	0.6827	6.90507	25.4739
47	7	400	50	3	150	0.3	3.93	1.91	4.002	1.9634	-0.072	-0.0534	-1.8321	-2.7958
48	5	220	50	2	150	0.3	6.86	1.89	6.0937	2.0668	0.7663	-0.1768	11.1706	-9.3545
49	7	150	50	3	150	0.3	5.28	2.1	4.993	2.0032	0.287	0.0968	5.43561	4.60952
50	3	220	55	2	150	0.15	3.95	1.13	4.6401	1.2329	-0.6901	-0.1029	-17.471	-9.1062
51	5	220	45	3	150	0.15	4.12	1.19	4.0588	2.0743	0.0612	-0.8843	1.48544	-74.311
52	7	220	45	2	150	0.15	7.41	2.16	7.0509	1.9744	0.3591	0.1856	4.84615	8.59259
53	5	220	50	2	150	0.3	7.11	2.15	7.0937	2.0668	0.0163	0.0832	0.22925	3.86977
54	7	220	55	2	150	0.15	6.68	2.23	6.6069	2.3228	0.0731	-0.0928	1.09431	-4.1614

There are several stages to follow when using a feed-forward network to build a neural model. One of the steps to be undertaken is to generate a dataset that needs to be trained and tested for the given network. In the present case, the dataset comprises the 54 observations from the design of experimental model of RSM. This dataset usually comprises input and target vectors paired across each other.[67] In this research work the neural network has been modeled and trained in MATLAB 2016b working environment.

3.2.1 *Neural model simulation for MRR*

As depicted in Figure 6, the neural simulation results nearly coincide with the corresponding experimental observations. In a sense, the neural model has been able to faithfully capture the experimental outputs.

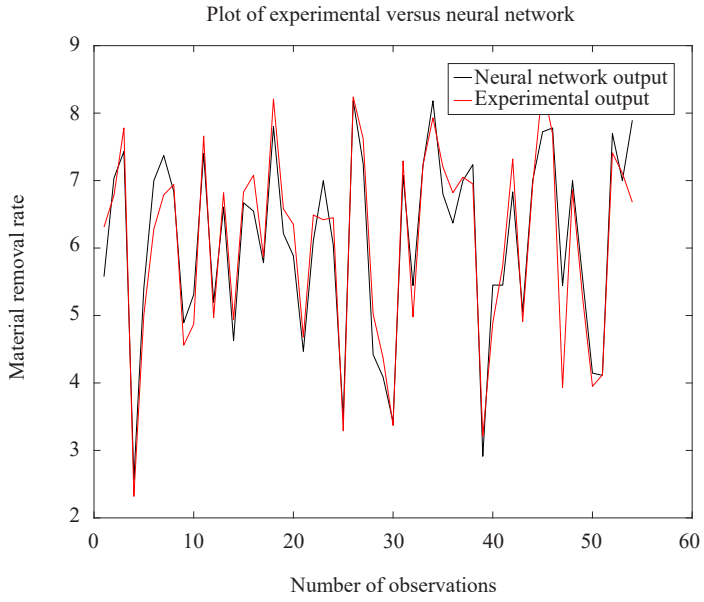

Figure 6. Plot of neural model simulation for MRR

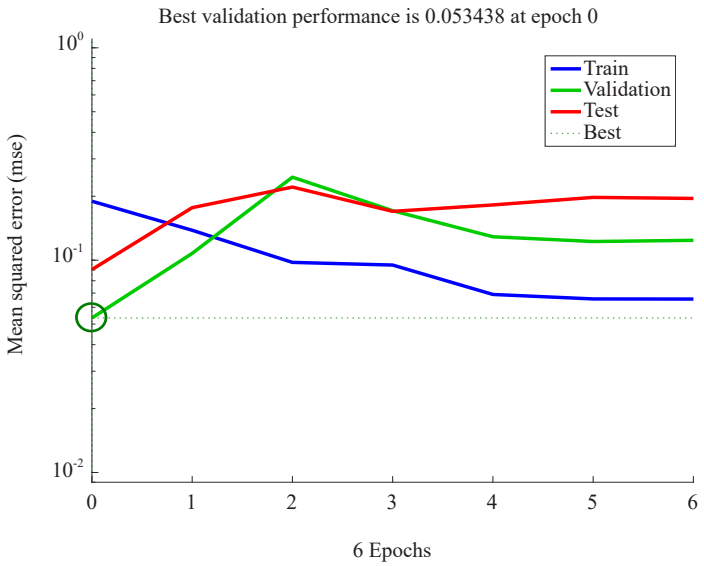

Figure 7. Training performance plot for MRR

The plot (Figure 7) depicts the performance of neural network training using the Bayesian Regularization function. In the plot shown in Figure 7, the training curve coincides with the best value after the start of the iteration. So, the neural model possesses the best training performance achieved after only 0 iterations, thus achieving a mean square error (MSE) of 0.053438.

The plot (Figure 8) of training state indicates the squared error dynamics corresponding to the entire dataset on a logarithmic scale. The low gradient value of 0.016141 pertains to back-propagation gradient at each epoch. A lower value implies the attainment of the bottom of the local minimum of the objective function. The validation checks correspond to the iterations whenever the MSE has an increased value. A low value of zero indicates that the neural model is perfectly trained.

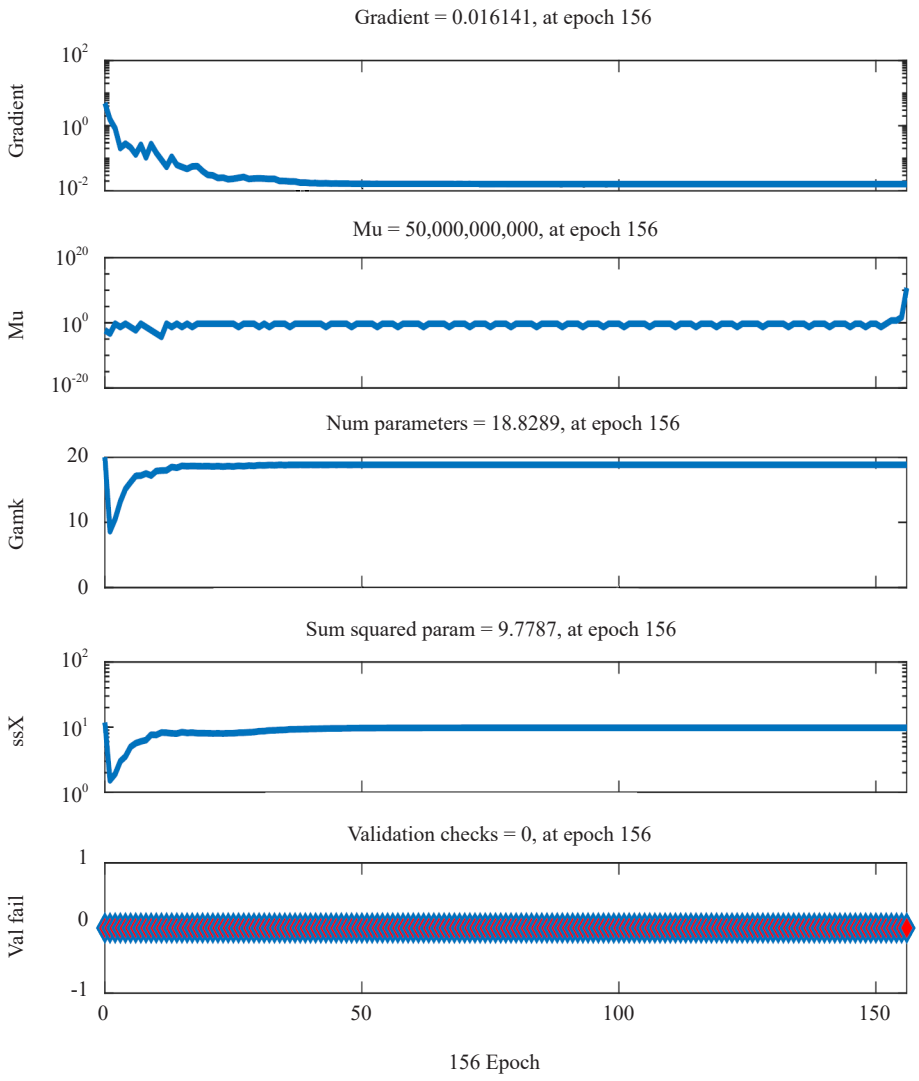

Figure 8. Training state plot of neural model for MRR

The y-label of the regression plot (Figure 9) denotes the equation thus signifying the mathematical relation between predicted and target values. Here these equations indicate how well this multi-layer perceptron (MLP) network is able to perform. It has two terms:

(1) The optimal value of the target coefficient for maximum logistic regression performance is close to 1. A perfectly acceptable present value would be 0.98686.

(2) The error residue, frequently expressed as a constant, is the second term and it must be added to the scaled goal in order to make it closer to the projected output. A value close to zero would be optimal under these circumstances. This value of 0.097 is virtually non-existent in the current plots (Figure 9).

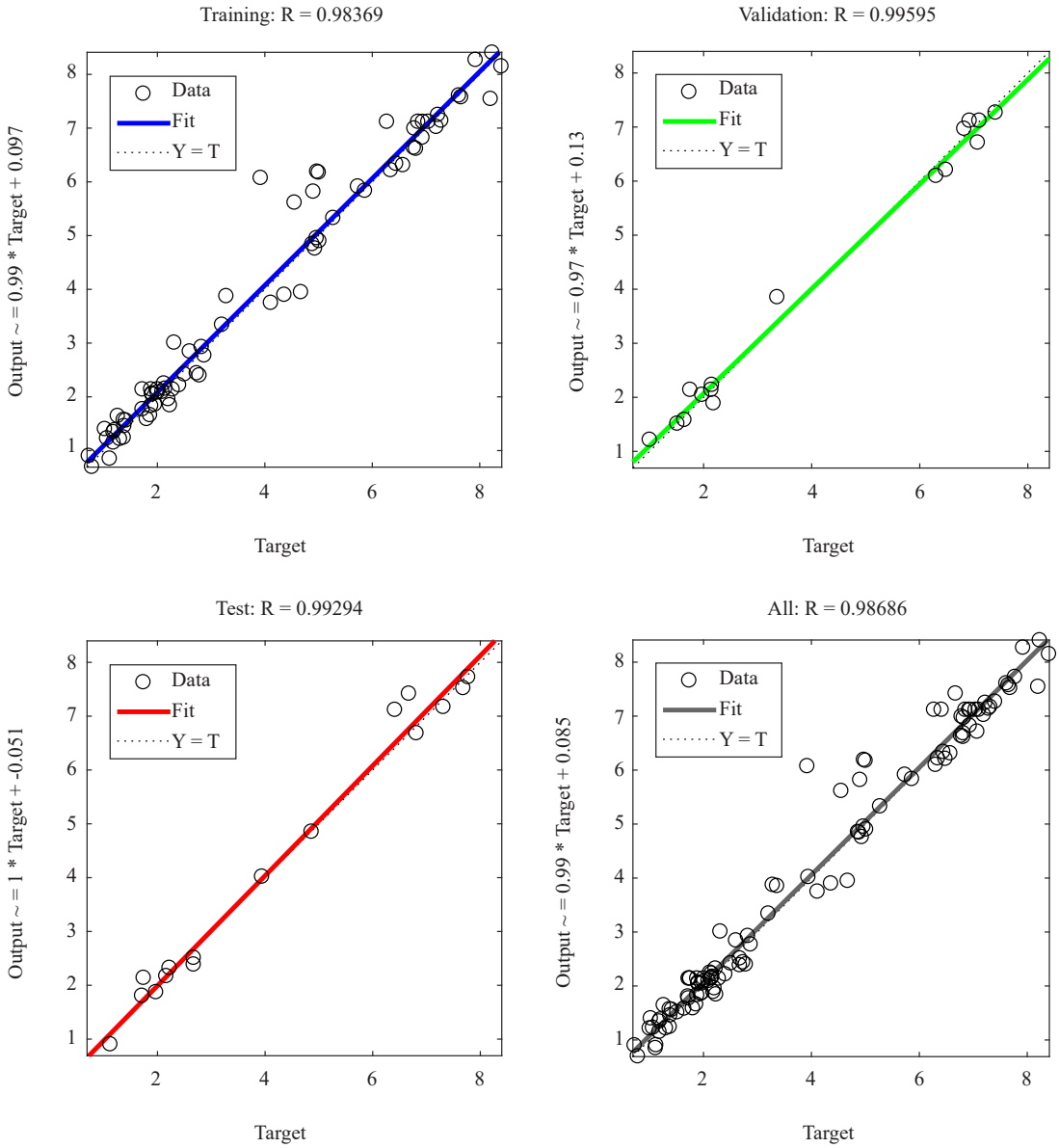

Figure 9. Regression plot of neural model for MRR

3.2.2 *Neural model simulation for ΔR_a*

Figure 10 depicts the near exact capturing of the experimental values by the proposed neural model. In Figure 11, the plot depicting the training performance, the minimum error value of 0.4926 is obtained at 6 training epochs. It is observed that the test variations swiftly converge with the best value line. Such results show that the neural model has been well trained.

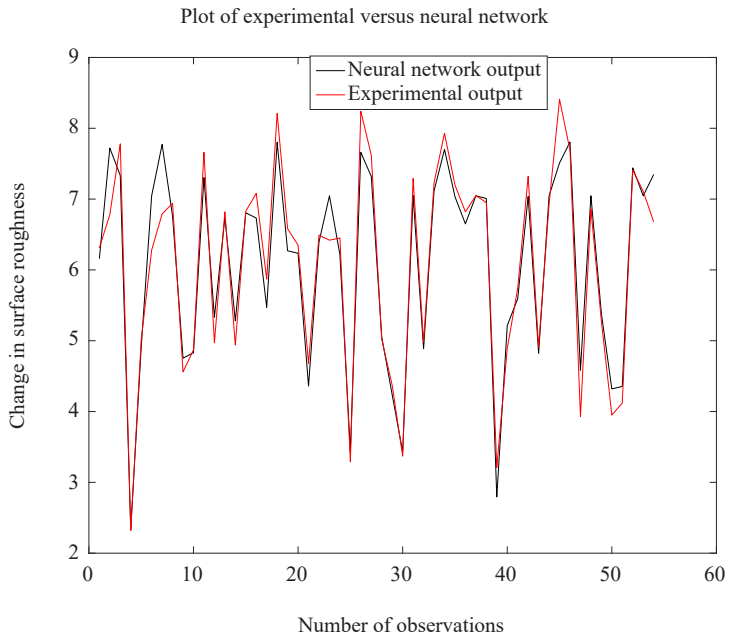

Figure 10. Plot of neural model simulation for ΔR_a

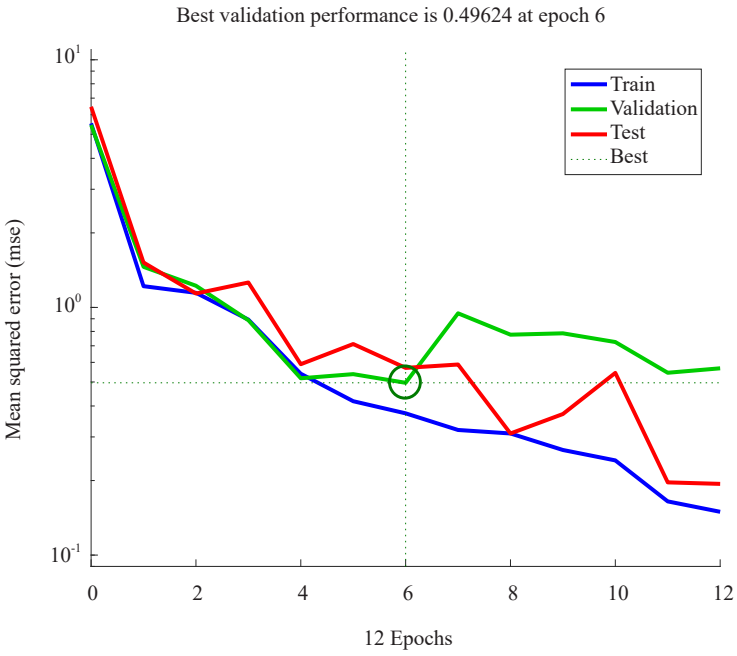

Figure 11. Training performance plot for ΔR_a

In Figure 12, the gradient value pertains to a low value of 0.01512, thus reaching the bottom of the local minimum of the objective function. On a similar basis, the zero count of the validation check indicates the near excellent training of the neural model.

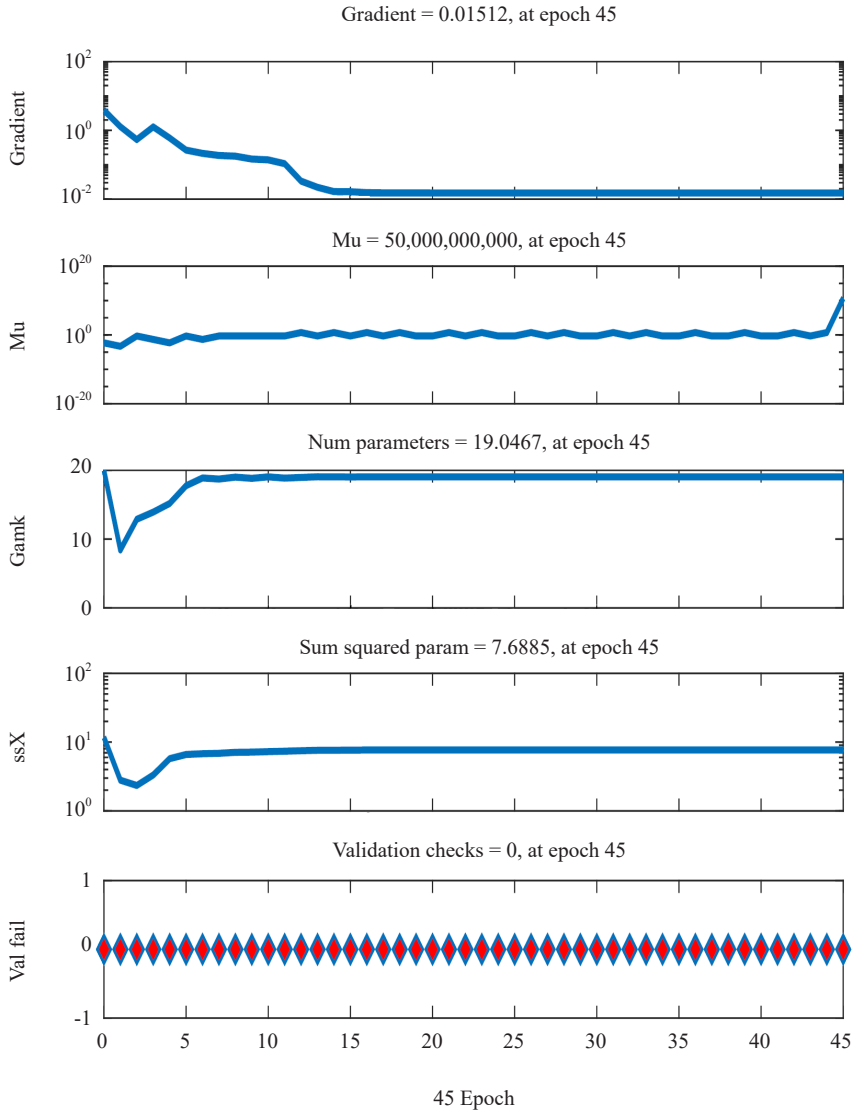

Figure 12. Training state plot of neural model for ΔR_a

In Figure 13, the target coefficient has a near unity value of 0.94, thus pertaining to good performance of the MLP network. The Second value of 0.26 is a near zero value and this indicates the literal matching of the scaled target with the predicted output value.

3.3 *Evaluation of experimental and ANN predicted values*

The predicted and experimental values of the neural model corresponding to MRR and ΔR_a correlate with a high degree with regard to each other. This is clearly visible in Figures 14 and 15. The maximum error for the neural model-predicted and experimental values for MRR and ΔR_a comes out to 13.51%, and 39.32%, respectively. Figures 14 and 15 clearly depict the inter-mingling of the plots of ANN and experimental results. It seems as if both the plots are superimposed on each other. Figure 14 depicts MRR parameter being simulated on the neural model while Figure 15 takes ΔR_a as a varying parameter.

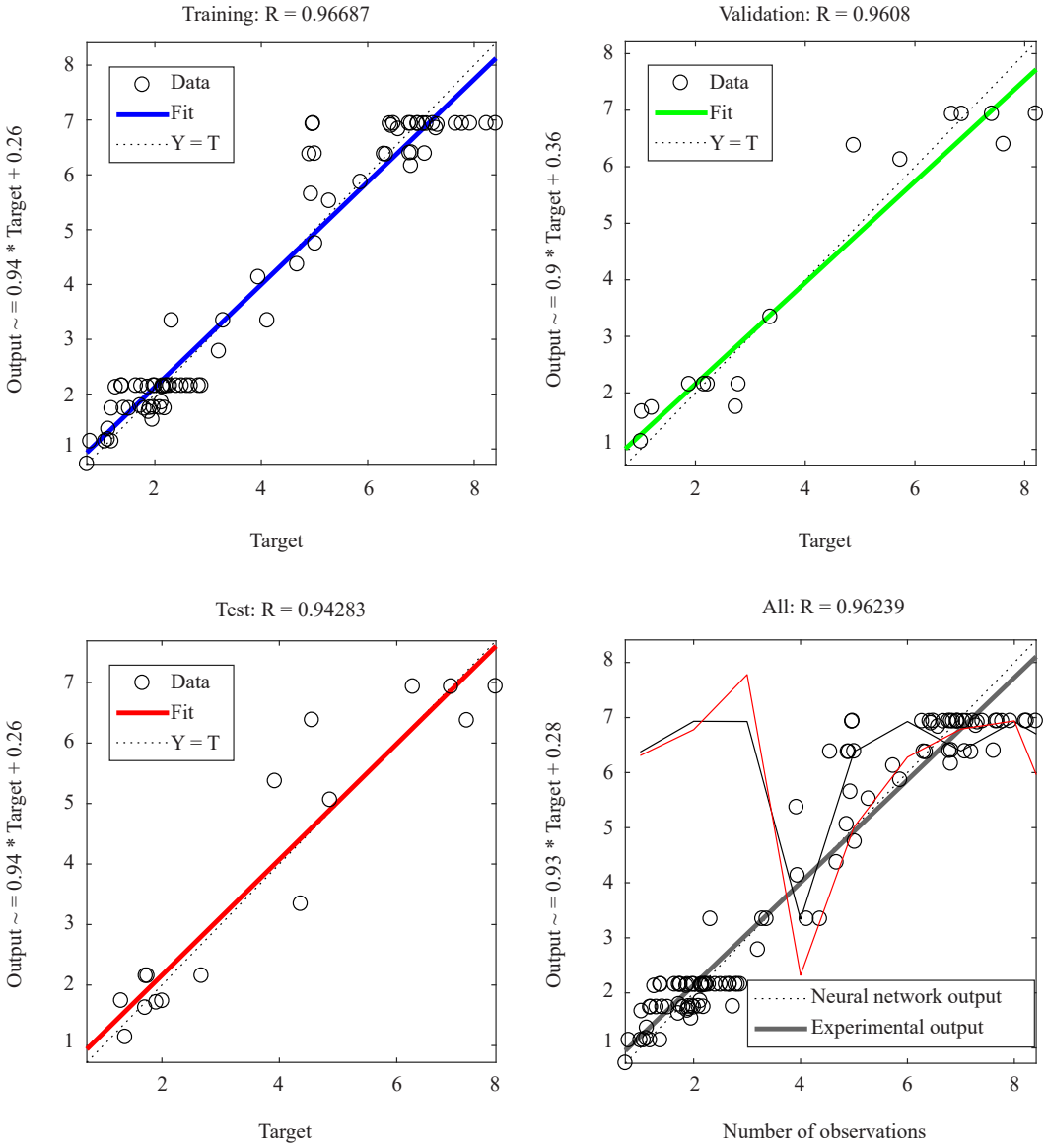

Figure 13. Regression plot of neural model for ΔR_a

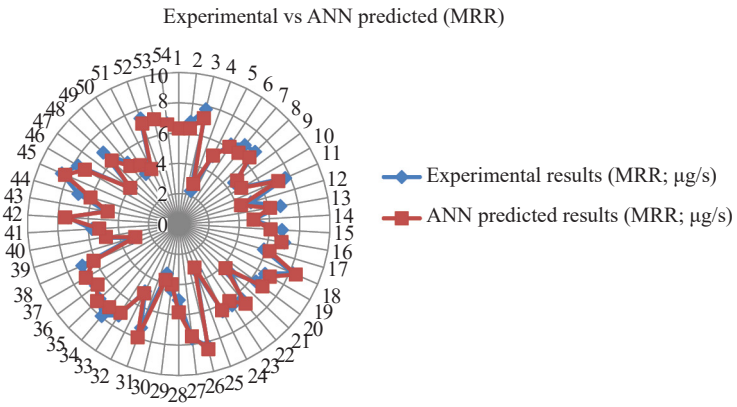

Figure 14. Graphical representation of experimental and ANN predicted results for MRR

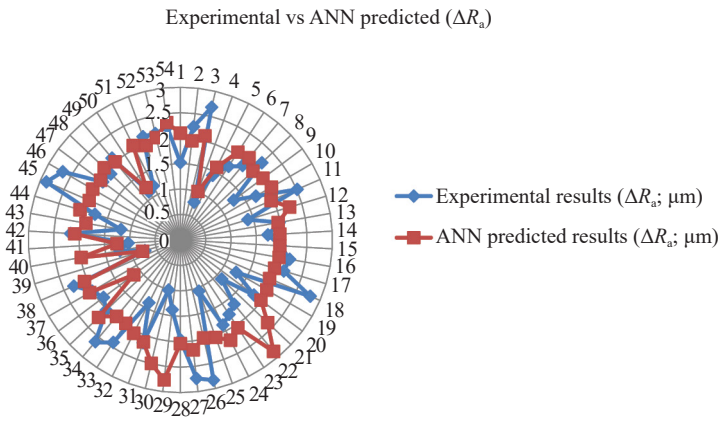

Figure 15. Graphical representation of experimental and ANN predicted results for ΔR_a

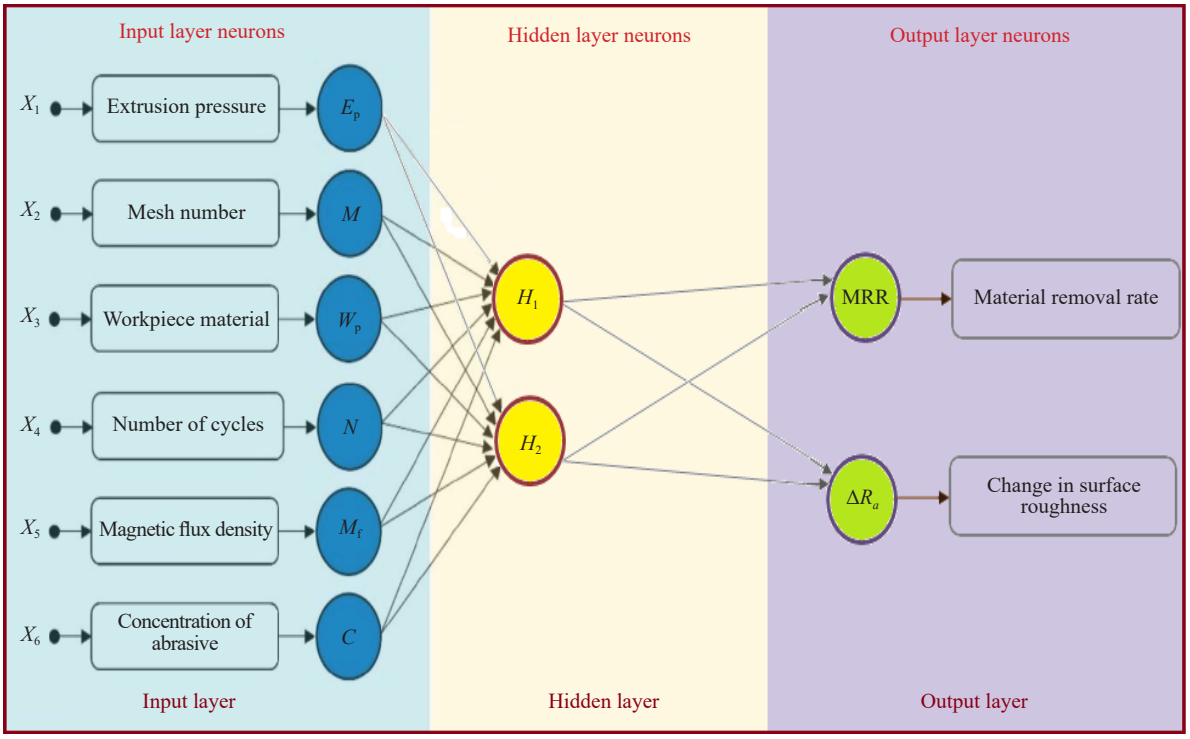

Figure 16. ANN architecture

3.4 *Proposed neural network architecture and error calculation*

The network architecture of the proposed neural model is diagrammatically represented in Figure 16. The input layers of the ANN model have 6 inputs namely E_p, M, C, W_p, N and M_f. The present configuration contains two hidden layers. These are chosen on the basis of the mean square error (MSE) coefficient at a minimal value. Figure 16 also depicts the outputs as MRR and ΔR_a. The quantity of the hidden layers and neurons in each hidden layer were chosen for a minimum MSE.

The efficiency of the neural network has been computed in terms of percentage error. The percentage error has been computed as per equation (5). The values obtained based on these calculations are shown in Table 7. It can be concluded

that the relation which exists among the input values and model outputs is trained through ANN model.

$$\text{Percentage error} = \frac{(\text{Experimental value} - \text{ANN predicted value})}{\text{Experimental value}} \times 100 \quad (5)$$

3.5 *Error plots*

The MRR of the MAFM process is represented by the neural model outputs overlaid against their investigational counterparts in Figure 17. It is also depicted that the error values fall within a limited range. Additionally, the results of the experimental study and the neural model almost match closely.

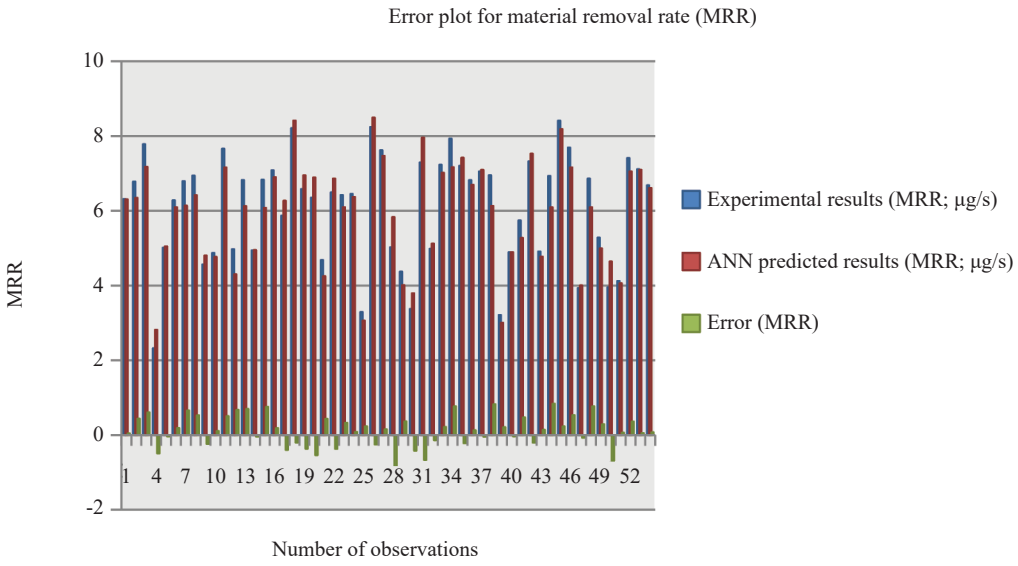

Figure 17. Error plot for MRR

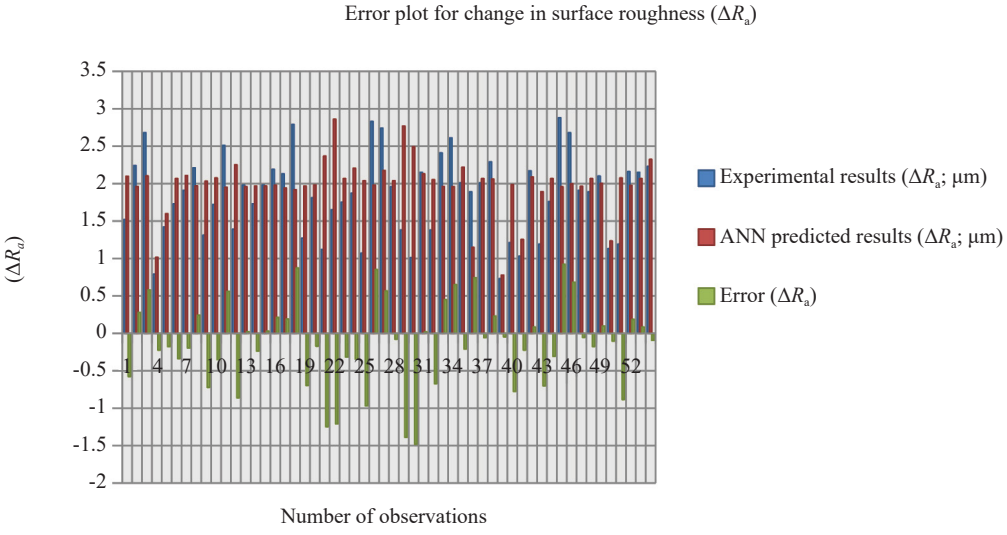

Figure 18. Error plot for ΔR_a

Figure 18 depicts the ΔR_a values for the experimental and neural model, respectively. The low error values in Figure 18 suggest that the neural model has been validated in comparison to the experimental data. The neural model outputs are observed to vary in accordance with the experimental values.

3.6 *Plot of mean square error*

The MSE is then represented as a bar plot (Figure 19) for the values obtained under different optimization techniques.

Figure 19. Mean square error plot

This is based on the learning rate parameter of the neural network. This parameter is optimized using algorithms of particle swarm optimization (PSO), genetic algorithm (GA), simulated annealing (SA) and pattern search (PS). The numerical values of mean square (MSE) have been tabulated in Table 8. Table 8 clearly indicates the minimum values obtained after optimizing the MSE, from the SA algorithm. Moreover, the optimized values obtained from GA and PS algorithms are quite close.

Table 8. Modeling error reduction by parameter optimization techniques

Coefficient type	Experimental	Particle swarm optimization (PSO)	Genetic algorithm (GA)	Simulated annealing (SA)
Mean square error	4.1919	1.3575	1.9225	1.3561

4. Microstructure analysis

In the engineering fields, surface morphology is used in hybrid materials to depict the critical response. After machining, the MAFM specimens have been analyzed using a scanning electron microscope (SEM) (JSM-6510LV, JEOL, USA). Before the SEM could be analyzed, the workpiece was cut into two pieces for taking SEM snaps of the processed surface and each specimen was washed with an acetone [$(CH_3)_2CO$] solution and then air dried. The magnification is done by a factor of 300. Due to the boring process used to prepare the cylindrical samples of Al-6063/SiC/B4C-MMCs, the inner surfaces of the unfinished specimen are quite rough. Before MAFM process, the detection results are shown in Figures 20. After MAFM process, the results detection are depicted in Figures 21 and

22 respectively. According to SEM micrograph analysis, the specimen surface witnessed some casting defects and irregularities such as cracks, craters, deep boring tool marks, scratches, multi-layers, micro, and big pits before the surfaces were machined using MAFM, as shown in Figures 20(a), 21(a) and 22(a). As per the SEM findings, the MAFM process revealed fine surface textures. Because of this, the outliers were drastically cut down. There were just a few embedded abrasive particles and abrasive grain markings, as illustrated in Figures 20(b), 21(b) and 22(b).

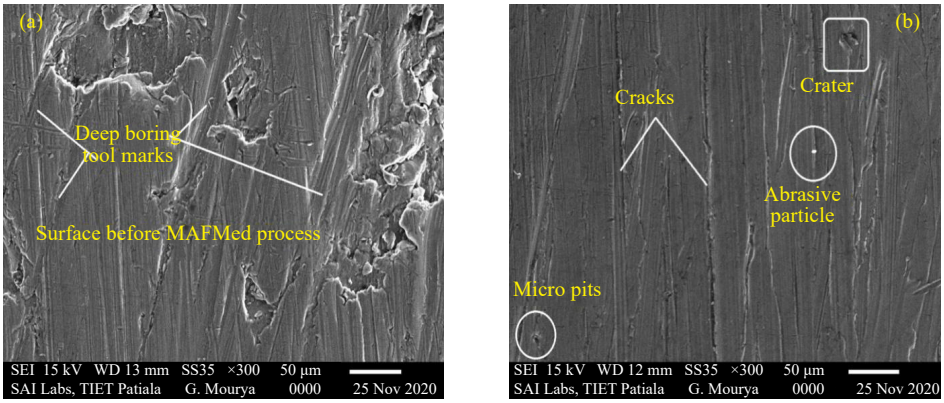

Figure 20. SEM micrograph of (a) unfinished and (b) finished Al-6063/SiC (9 wt. %)/B_4C (1 wt. %)-MMC (workpiece-1)

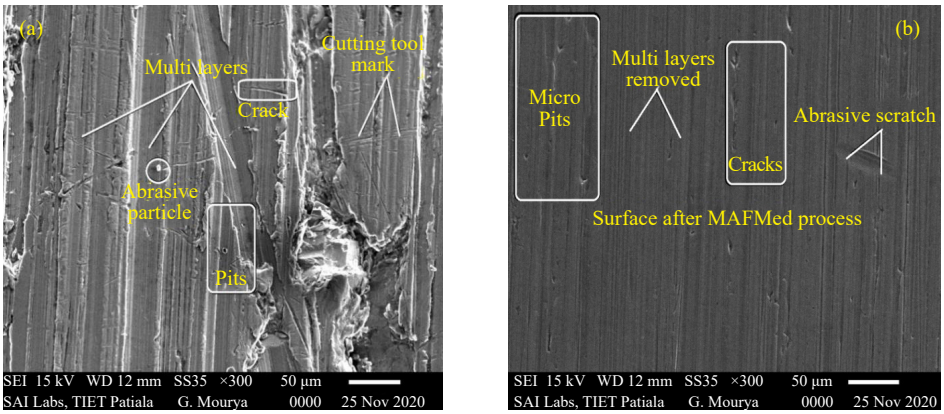

Figure 21. SEM micrograph of (a) unfinished and (b) finished Al-6063/SiC (8 wt. %)/B_4C (2 wt. %)-MMC (workpiece-2)

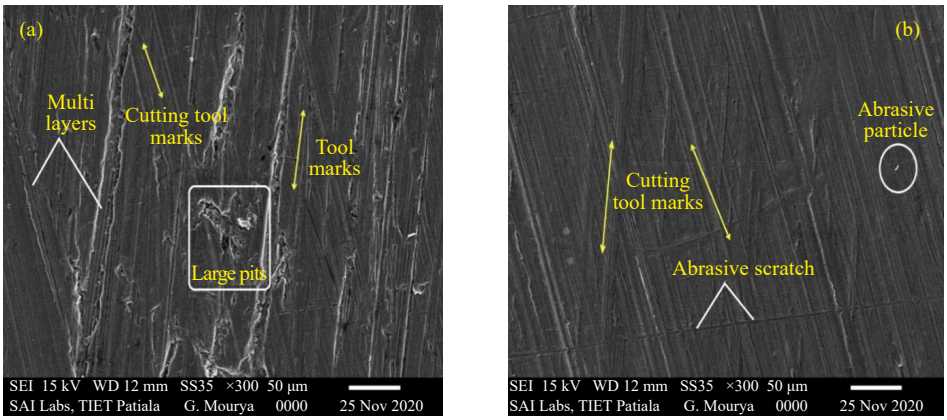

Figure 22. SEM micrograph of (a) unfinished and (b) finished Al-6063/SiC (7wt. %)/B_4C (3 wt. %)-MMC (workpiece-3)

5. Optimization methods for neural modelling parameters

5.1 *Neural simulated parameter optimization using genetic algorithm (GA)*

Algorithms employed for optimizing the parameters are categorized as intelligent procedures used for the evaluation of optimal machining conditions.[68] The techniques of ANN and genetic algorithms (GA) broadly can be classified as evolutionary optimization methods. These methods have been applied in typical objective function problems.[69-73] The following steps are initiated in the optimization using GA:

(1) Setting up the GA parameters constitutes specification of size of population and number of generations. Also, the decision has to be taken on upper and lower limits for the process variables.

(2) Creation of first random sample.

(3) Assessing the level of fitness for every individual.

(4) After the previous stage the GA is put into action.

(5) The generation count is incremented at each stage.

(6) The process terminates, in case the current generation count exceeds the maximum count of generations.

(7) If the previous step does not work, the process moves to step (3).

5.2 *Parameter optimization using simulated annealing (SA)*

It represents the process of metal annealing which consists of re-structuring the metal with minimal energy. This happens when the metal is allowed to cool in a slow fashion, after the heating.

It consists of the following steps:

(1) Start with an initial state z.

(2) Generate a new neighboring state $\underline{z}$.

(3) Compute the target function E_1 corresponding to state z.

(4) Calculate the target function E_2 corresponding to state $\underline{z}$.

(5) Get the difference $\Delta E = E_1 - E_2$.

(6) If the energy is higher, then the new state is accepted with the probability given by:

$$P_z = \exp\left(-\frac{\Delta E}{kT}\right)$$

(7) In case the resulting energy is lower, the new state is accepted with minimal energy E.

(8) The probability computed in step (6) assumes maximal value, for the states having minimal E for lower temperature T (near to zero value).

(9) For the above case, the system assumes a relaxed state corresponding to the global minima.

Following the above steps, the minimization of the error has been implemented using the SA algorithm in this paper.[74]

5.3 *Parameter optimization using particle swarm optimization (PSO)*

Nature-inspired algorithms owe their popularity, in the research circles, to the efficacy in evaluating the objective function. These algorithms are free from the derivatives thus obviating the need to calculate the numerical derivatives of the objective function.[74]

The PSO algorithm is inspired by the behavior of animals in groups. It could include intelligence exhibited by a swarm of fish, birds or maybe even humans.[75-76]

The following steps are required:

(1) Each group (or swarm) is presented as a point in the Cartesian system.

(2) Thereafter, the point above is assigned with a value of particle position (x^i), previous best position (p^i) and initial velocity (v^i).

(3) Evaluate the fitness of each particle F (x^i).

(4) Compute the fitness of previous best particle position $F(p^i)$.

(5) In case the fitness value is lower than the previous particle i.e. $F(x^i) < F(p^i)$, then

(6) Save this current particle position i.e. $p^i = x^i$

(7) As the fitness values of all particles were lower than the current best solutions i.e. $F(x^i) < F(G)$, where G is the global best position.

(8) The previous best positions are now the particle positions having better values. So, all the positions need to be updated as per the equation:

$$x^i(t+1) = x^i(t) + v^i(t+1)$$

(9) Each particle moves to the next position by updating the velocity.

(10) Due to this, the best solutions corresponding to the new positions were also updated.

(11) Compute the optimal position of each individual.

(12) Calculate the optimal position of the whole swarm.

(13) The PSO algorithm makes use of the above variables to search for the best solution in the area. The position and velocity of the particles are updated after each iteration, to attain the condition, defined by the stopping criterion.

6. Future directions

The present research work focuses on the application of the aluminium composites in the MAFM process. However, the quality of research[77-86] as well as the future outcomes can be enhanced, if the following measures can be adopted to achieve results in new directions:

(1) According to the literature, various AFM processes have been used to finish homogeneous materials such as aluminium, mild steel, brass, copper, gun-metal, Ti-6Al-4V titanium alloy, stainless steel (SUS-304), stainless steel (202), AISI stainless steel (316L), AISI 52100 steel, AISI 1045, 1080, and A36 steels. The current research is an attempt to use MAFM to investigate the machinability features of hybrid Al/SiC/B_4C-MMCs. Considering the huge potential of this approach, there is still a need for more research. The study could be expanded to include the heterogeneous materials such as Al/SiC/BN_3, Al/SiC/CNT, Al/SiC/CBN, Al/SiC/AlN, Al/SiC/Graphite, Al/SiC/Zirconia, etc.

(2) During the MAFM process, one can examine how several other process factors such as media viscosity, media flow speed, oil concentration in media, working gap, finishing time, electromagnet voltage and current, etc. impact MRR and ΔR_a.

(3) The analysis of media characteristics is one of the challenging areas that further needs to be explored by varying process parameters.

(4) Although the current research work on parametric optimization of the MAFM process through neural networks approach has been aptly studied, there is still room for more research. To examine and compare the results, other optimization approaches such as machine learning algorithms, fuzzy logic, lion optimization algorithm, ant colony optimization and others can be employed.

(5) The sustainability of the MAFM process can be enriched by finishing complex geometries, unsymmetrical and free form surfaces, to gain more insights.

(6) A generalized mathematical model for MAFM can be developed to obtain the outcomes in order to assess the parametric effect through Finite Element Method (FEM).

7. Conclusion

In this paper, the process of MAFM has been investigated in the paradigm of machining parameters and the material composites. The paper analyzes the effectiveness of the machining parameters. Here, the research work has been carried out, with a multi-objective approach. Firstly, the experimentation on the abrasive flow machining is done by introducing the magnetic field around the workpiece, to enhance the material removal rate, achieved during the

surface finish. The SEM morphology of Al/SiC/B_4C examination of the finished surfaces revealed the improved surface finish of the workpiece. Numerous irregularities and casting defects such as cracks, multi layers, micro and large pits, voids and cutting tool marks have been deteriorated or integrated with the irregular debris or craters after finishing with the MAFM process. The surface topography of the machined sample has been greatly enhanced.

The experimental parameters have been obtained using the Design of Experiments software. In the present work, the MAFM process is investigated using the hybrid ANN approach. As a result, the neural network method is employed to mimic the connectivity between experimentally obtained model parameters. As such, the modeling error computed from the neural simulation parameters, is significant enough. Hence it becomes imperative to minimize its magnitude by the application of nature-inspired optimization techniques like particle swarm optimization, genetic algorithms and the simulated annealing. The resulting model parameters are observed to drastically reduce using the above optimizing methods. The neural network training has achieved a minimal training error of 0.053438 and 0.49624 corresponding to MRR and ΔR_a respectively, as observed through the network training plot. The regression plots depict the excellent agreement between the experimental and model parameters as a factor value of 0.98686 and 0.96239 corresponding to MRR and ΔR_a respectively, which can be considered as closer to 1. The model parameters have been reduced to the minimal using the methods of GA, SA and PSO and pattern search discussed earlier. Though these are the powerful methods in optimization, the simulated annealing (SA) method has outperformed and has proved to be the most efficient and has reduced the error by 67.645%.

Funding

The author(s) received no financial support for the research, authorship, and/or publication of this article.

Conflict of interest

The authors declare that they have no conflict of interest.

References

[1] Rhoades, L. J. In *Abrasive flow machining and its use*, Proceedings of Non Traditional Machining Conference; Cincinnati, OH, 1985; pp 111-120.
[2] Rhoades, L. J. *SME Technical Paper MR 85-475*; Society of Manufacturing Engineers: Dearborn, MI, USA, 1985; pp 1-18.
[3] Perry, W. *SME Paper MR75-831*; Society of Manufacturing Engineers: Dearborn, MI, USA, 1975.
[4] Stackhouse, J. *SME Paper MR75-484*; Society of Manufacturing Engineers: Dearborn, MI, USA, 1975.
[5] Kohut, T. In *Surface finishing with abrasive flow machining*, Proceedings of Fourth International Aluminum Extrusion Technology Seminar; Washington, DC, 1988; pp 35-43.
[6] Williams, R. E.; Rajurkar, K. P. *SME Paper FC89-806*; Society of Manufacturing Engineers: Dearborn, MI, USA, 1989; pp 898-906.
[7] Williams, R. E.; Rajurkar, K. P. *Trans. ASME, J. Eng. Ind.* **1992,** *114*, 74-81.
[8] Loveless, T. R.; Rajurkar, K. P.; Williams, R. E. *J. Mater. Process. Tech*. **1994,** *47*, 133-151.
[9] Kozak, J.; Rajurkar, K. P.; Williams, R. E. *Trans. NAMRI/SME* **1992**, *20*, 145-150.
[10] Fletcher, A. J.; Davies, P. J. *Proc. Instn. Mech. Engrs*. **1995,** *209*, 409-418.
[11] Fletcher, A. J. In *Computer modeling of the abrasive flow machining process*, Proceedings of International Conference on Surface Engineering; Toronto, Canada, 1990; pp 592-601.
[12] Wang, Z.; Geng, X.; Chi, G.; Wang Y. *Mater. Manuf. Process.* **2014,** *29*, 532-539.
[13] Przyklenk, K. *ASME-PED: Adv. Non-Trad. Machining* **1986,** *22*, 101-110.
[14] Jain, V. K.; Jain, R. K. *Int. J. Mach. Tool Manuf*. **1999,** *39*, 1903-1923.
[15] Jain, V. K.; Adsul, S. G. *Int. J. Mach. Tools Manuf*. **2000,** *40*, 1003-1021.
[16] Lam, S. S. Y.; Adsul, S. G. In *Process monitoring of abrasive flow machining process using neural network model*,

Proceedings of 6th Industrial Engineering Research Conference; Miami Beach, FL, 1997; pp 477-482.
[17] Wang, A. C.; Weng, S. H. *J. Mater. Proc. Tech*. **2007,** *192-193*, 486-490.
[18] Sankar, M. R.; Jain, V. K.; Ramkumar, J.; Josh, Y. M. *Int. J. Mach. Tools Manuf*. **2012,** *51*, 947-957.
[19] Steif, P. S.; Haan, J. J. *Wear* **1998,** *219*, 177-183.
[20] Jones, A. R.; Hull, J. B. *Ultrasonics* **1998,** *36*, 97-101.
[21] Gilmore, J. R. *Orbital Polishing-An Emerging Technology*; SME Buff and Polish Clinic, Schaumburg, IL, 1997.
[22] Ahmad, S.; Singari, R. M.; Mishra, R. S. *Mater. Manuf. Process*. **2021,** *36*, 843-857.
[23] Sharma, M.; Janardhan, G.; Sharma, V. K.; Kumar, V.; Joshi, R. *J. Proc. Mech. Engg*. **2022,** *236*, 790-804.
[24] Oh, J. H.; Lee, S. H. *Proc. Inst. Mech. Engineers, Part B: J. Engg. Manuf*. **2010,** *225*, 853-865.
[25] Djavanroodi, F. *Research J. App. Sci., Engg. Tech*. **2013,** *6*, 1976-1983.
[26] El-Sonbaty, I. A.; Khashaba, U. A.; Selmy, A. I.; Ali, A. I. *J. Mater. Proc. Tech*. **2008,** *200*, 271-278.
[27] Abburi, N. R.; Dixit, U. S. *Robot. Comput.-Integr. Manuf*. **2006,** *22*, 363-372.
[28] Jain, R. K.; Jain, V. K.; Kalra, P. K. *Wear* **1999,** *231*, 242-248.
[29] Lam, S. S. Y.; Smith, A. E. *Cascade-Correlation Neural Network Modeling of the Abrasive Flow Machining Process* [Online]. https://www.eng.auburn.edu/~aesmith/files/ijie98.pdf (accessed May 14, 2024).
[30] Teimouri, R.; Baseri, H. *J. Mech. Sci. Tech*. **2013,** *27*, 533-539.
[31] Sankar, M. R.; Mondal, S.; Ramkumar, J.; Jain, V. K. *Int. J. Adv. Manuf. Tech*. **2008,** *42*, 678-688.
[32] Jain, R. K.; Jain, V. K. *J. Mater. Proc. Tech*. **2000,** *108*, 62-67.
[33] Rajurkar, K. P.; Kozak, J. *Hybrid Machining Process Evaluation and Development* [Online]. https://wn.com/Unl/news (accessed May 14, 2024).
[34] Shinmura, T.; Yamaguchi, H. *JSME Int. J., Ser. C* **1995,** *38*, 798-804.
[35] Kremen, G. Z.; V Elsayed, E. A.; Rafalovich, I. *Int. J. Prod. Res*. **1996,** *34*, 2629-2638.
[36] Kim, J. D. *J. Mater. Proc. Tech*. **1997,** *71*, 384-393.
[37] Khairy, A. B. In *Aspects of surface and edge finishing by magneto abrasive particles*, Proceedings of International Conference on Advanced Manufacturing Technology; Malaysia, 2000; pp 77-84.
[38] Shan, H. S.; Singh, S. *Int. J. Mach. Tools Manuf*. **2002,** *42*, 953-959.
[39] Chaurasia, A.; Rattan, N.; Mulik, R. S. *J. Braz. Soc. Mech. Sci. Eng*. **2018,** *40*, 1-10.
[40] Kataria, M.; Mangal, S. K. *J. Braz. Soc. Mech. Sci. Eng*. **2019,** *41*, 1-13.
[41] Kumar, M.; Das, M.; Yu, N. *J. Braz. Soc. Mech. Sci. Eng*. **2022,** *205*, 1-15.
[42] Sirwal, S. A.; Singh, A. K.; Paswan, S. K. *J. Braz. Soc. Mech. Sci. Eng*. **2020,** *140*, 1-23.
[43] Zhang, S.; Long, Z.; Yang, X. *J. Braz. Soc. Mech. Sci. Eng*. **2021,** *56*, 1-10.
[44] Singh, R. K.; Gangwar, S.; Singh, D. K.; Pathak, V. K. *J. Braz. Soc. Mech. Sci. Eng*. **2019,** *270*, 1-19.
[45] Ali, P.; Walia, R. S.; Murtaza, Q.; Singari, R. M. *J. Braz. Soc. Mech. Sci. Eng*. **2020,** *302*, 1-28.
[46] Heng, L.; Kim, J. S.; Song, J. H.; Mun, S. D. *J. Mater. Res. Tech*. **2021,** *15*, 3268-3282.
[47] Verma, G. C.; Kala, P.; Pandey, P. M. *Int. J. Adv. Manuf. Tech*. **2016,** *88*, 1657-1668.
[48] Azizi, A.; Khoshanjam, A.; Bahrami, P.; Khoshanjam, K. *Proc. Inst. Mech. Eng., Part B: J. Engg. Manuf*. **2023,** *237*, 338-349.
[49] Judal, K. B.; Yadava, V.; Pathak, D. *Mater. Manuf. Process.* **2013,** *28*, 1196-1202.
[50] Kala, P.; Kumar, S.; Pandey, P. M. *Mater. Manuf. Process*. **2013,** *28*, 200-206.
[51] Kala, P.; Pandey, P. M. *Procedia Mater. Sci*. **2014,** *5*, 1677-1684.
[52] Finnie, I. *Wear* **1972,** *19*, 81-90.
[53] Rabinowicz, E. *Wear* **1961,** *4*, 345-355.
[54] Neilson, J. H.; Gilchrist, A. *Wear* **1968,** *11*, 111-122.
[55] Kumar, A.; Kumar, V.; Kumar, J. *Proc. IMechE Part B: J. Engg. Manuf*. **2013,** *227*, 972-992.
[56] Prabhu, S.; Uma, M.; Vinayagam, B. K. *J. Braz. Soc. Mech. Sci. Eng*. **2014,** *36*, 637-652.
[57] Dash, L.; Padhan, S.; Das, S. R. *J. Braz. Soc. Mech. Sci. Eng*. **2020,** *500*, 1-25.
[58] Cochran, G.; Cox, G. M. *Experimental Design*; Asia Publishing House: New Delhi, 1962.
[59] Peruri, S. R.; Chaganti, P. K. *J. Braz. Soc. Mech. Sci. Eng*. **2019,** *450*, 1-17.
[60] Qian, C.; Fan, Z.; Tian, Y.; Liu, Y.; Han, J.; Wang, J. *Int. J. Adv. Manuf. Tech*. **2020,** *112*, 1-16.
[61] Souza, A. M.; da Silva, E. J.; Ratay, J.; Yamaguchi, H. *J. Braz. Soc. Mech. Sci. Eng*. **2022,** *327*, 1-17.
[62] Mangal, S. K.; Sharma, V. *J. Braz. Soc. Mech. Sci. Eng*. **2017,** *39*, 4191-4206.
[63] Arora, K.; Singh, A. K. *J. Braz. Soc. Mech. Sci. Eng*. **2021,** *43*.
[64] Dixit, N.; Sharma, V.; Kumar, P.; Yamaguchi, H. *J. Manuf. Process*. **2021,** *64*, 1434-1461.
[65] Aggarwal, A.; Singh, A. K. *J. Braz. Soc. Mech. Sci. Eng*. **2021,** *43*, 444.

[66] Hornik, K.; Stinchcombe, K.; White, H. *Neural Netw*. **1989,** *2*, 359-366.
[67] Goodfellow, I.; Bengio, Y.; Courville, A. *Deep Learning*; MIT Press: Cambridge, MA, 2016.
[68] Paszkowicz, W. *Mater. Manuf. Process*. **2009,** *24*, 174-197.
[69] Pettersson, F.; Biswas, A.; Sen, P. K.; Saxena, H.; Chakraborti, N. *Mater. Manuf. Process*. **2009,** *24*, 320-330.
[70] Nakhjavani, O. B.; Ghoreishi, M. *Mater. Manuf. Process*. **2006,** *21*, 11-18.
[71] Sukhomay, P.; Pal Surjya, K.; Samantaray Arun, K. *Mater. Manuf. Process*. **2010,** *25*, 606-615.
[72] Somashekhar, K. P.; Ramachandran, N.; Jose, M. *Mater. Manuf. Process*. **2010,** *25*, 467-475.
[73] Zhang, F.; Tao, R.; Zhu, D. *J. Braz. Soc. Mech. Sci. Eng*. **2022,** *44*, 279.
[74] Leondes, C. T. *Optimization Techniques*; Academic Press: San Diego, 1998; pp 247-248.
[75] Eberhart, R.; Kennedy, J. In *A new optimizer using particle swarm theory*, Sixth International Symposium on Micro Machine and Human Science; IEEE: Nagoya, Japan, 1995; pp 39-43.
[76] Cao, G.; Wu, H.; Chu, Y. *J. Braz. Soc. Mech. Sci. Eng*. **2022,** *44*, 94.
[77] Manikandan, R.; Ponnusamy, P.; Nanthakumar, S.; Gowrishankar, A.; Balambica, V.; Girimurugan, R.; Mayakannan; S. *Materials Today: Proceedings* **2023**.
[78] Rampal, R.; Walia, A. S.; Somani, N.; Goyal, T.; Gupta; N. K. *Int. J. Interact. Des. Manuf.* **2024**.
[79] Dixit, N.; Sharma, V.; Kumar, P. *Mater. Manuf. Process*. **2023,** *38*, 1291-1306.
[80] Kaushik, A.; Singh, P.; Kumar, H.; Singh, L. *J. of Magn. Magn. Mater*. **2023,** *587*, 171294.
[81] Kumar, Y.; Singh, H.; Tandon, P.; Kuldeep; Basheed, G. A.; Barik, A.; Vishwakarma, P. N. *Wear* **2024,** *556-557*, 205528.
[82] Tian, Y.; Ma, Z.; Ahmad, S.; Qian, C.; Ma, X.; Yuan, X.; Fan, Z. *J. Manuf. Sci. Eng. Mar.* **2024,** *146*, 031002.
[83] Basha, S. M.; Sankar, M. R.; Venkaiah, N. *J. Manuf. Process*. **2024,** *131*, 844-860.
[84] Zhao, X.; Zhang, X.; Cheng, Bo; Li, W, Seniuts, U.; Viktor, Z. *Mater. Today Commun*. **2024,** *38*, 107901.
[85] Maurya, S. K.; Susheel, C. K.; Manna, A. *Int. J. Precis. Eng. Manuf*. **2024,** *25*, 1587-1600.
[86] Bhardwaj, A.; Ali, P. *Mapan-J. Metrol. Soc. India*. **2024,** *39*, 285-308.